Foundational Investigation of Electrophoretic Exclusion

by

Michael Keebaugh

A Dissertation Presented in Partial Fulfillment
of the Requirements for the Degree
Doctor of Philosophy

Approved November 2015 by the
Graduate Supervisory Committee:

Mark Hayes, Chair
Alexandra Ros
Daniel Buttry

ARIZONA STATE UNIVERSITY

December 2015

ABSTRACT

Electrophoretic exclusion is a counter-flow gradient focusing method that simultaneously separates and concentrates electrokinetic material at a channel entrance utilizing electric and fluid velocity fields. However, its effectiveness is heavily dependent on the non-uniform field gradients about the entrance. This work assesses the capability of electrophoretic exclusion to capture and enrich small molecules and examines the channel entrance region both quantitatively and qualitatively to better understand the separation dynamics for future design.

A flow injection technique is used to experimentally evaluate electrophoretic exclusion of small molecules. Methyl violet, a cationic dye, and visible spectroscopy are used to monitor flow and electrophoretic dynamics at the entrance region resulting in successful capture and simultaneous enrichment of methyl violet at the channel interface. Investigation of the entrance region is performed using both experiment data and finite element analysis modeling to assess regional flow, electric fields, diffusion, convection, and electrophoretic migration. Longitudinal fluid velocity and electric field gradient magnitudes near the channel entrance are quantified using Particle Tracking Velocimetry (PTV) and charged fluorescent microspheres. Lateral studies using rhodamine 123 concentration monitoring agree qualitatively with simulation results indicating decreased gradient uniformity for both electric and fluid velocity fields closer to the channel wall resulting in a localized concentration enhancement at lower applied voltages than previously observed or predicted. Resolution interrogation from both a theoretical assessment and simulation construct demonstrate resolution improvement with decreased channel width and placement of an electrode directly at the interface. Simulation

resolution predictions are in general agreement with early experimental assessments, both suggesting species with electrophoretic mobilities as similar as 10^{-9} $m^2/(Vs)$ can be separated with the current design. These studies have helped evolve the understanding of the interface region and set the foundation for further interface developments.

To Mom, for all that you gave.

ACKNOWLEDGMENTS

I would like to first thank my advisor, Dr. Mark Hayes for his guidance, patience, and flexibility throughout this journey. The willingness to help me no matter the time, day, or place was truly appreciated. I always enjoyed our interesting conversations that not only pertained to science, but to those other things in life as well. I must also recognize the School of Molecular Sciences and Graduate Education for the flexibility offered during the completion of my non-traditional graduate career.

I would also like to thank the former and current students of the Hayes' lab with whom I have had the pleasure of learning alongside. While the list of names is especially long given my tenure in this group, I would particularly like to thank Dr. Melissa McLaughlin, Dr. Michelle Meighan, Dr. Stacy Kenyon, and Dr. Paul Jones. Melissa - for the candor and enthusiasm during my exploration phase of graduate school, Michelle - for the positive attitude and project collaboration, Stacy - for the keen interpersonal awareness that I always appreciated, and Paul – for the words of encouragement, even if I knew I did a terrible job!

My desire to attend graduate school would have never been piqued had it not been for the research opportunities provided during my undergraduate years. I would therefore like to thank Dr. Brian Logue for the mentorship during my summer intern years, and Dr. Liwei Chen for the freedom and encouragement to explore my interests in his lab during my senior year. These opportunities helped me discover the thrill of obtaining data and interpreting results.

Completion of this degree would not have been possible without the love and support of my wonderful wife. Cortney was without a doubt the cornerstone during this

process. From giving birth to four beautiful children over the last five years to raising them often alone when I was at work, traveling, or in the lab, she continually displayed her strength, love, patience, and commitment toward our children and to me. She has been a remarkable wife, friend, and woman who deserves equal credit for the completion of this degree.

Finally, I would like to thank my family. Thank you to my sisters and their husbands for always visiting during the brief moments we would come home, and especially for the support given to the family when I could not be there. Thank you to my in-laws for the visits to Arizona when we needed help. Thank you to my Dad for demonstrating the value of a strong work ethic and attention to detail. And thank you Mom, especially for your kind-heartedness, your strength, and your never-ending encouragement; how I wish you could be here for this.

TABLE OF CONTENTS

Page

CHAPTER Page

LIST OF TABLES

LIST OF FIGURES

Figure Page

Chapter 1

Introduction

1.1 Bioanalytes and complex samples

Bioanalytes found in blood, urine, saliva, and other parts of the human body have the potential to provide a snapshot of individual health and disease states and offer a largely untapped resource in areas such as targeted treatments, drug design, and better understanding of biological pathways and function. In addition to pharmacology, toxicology, and biomedicine, the inherent value of robust analyte analysis extends to environmental, food, forensic, genetic, and many other industries and research institutions. However, these proteins, peptides, metabolites, DNA, RNA, and even the very cells that contain some of these information-rich components, often reside at low concentration in rather complex samples that can contain several thousand different components, thereby challenging even the most dynamic diagnostic tools [1] (Figure 1.1). For instance, even with significant advances in instrumentation, multidimensional fractionation, enrichment strategies, and high-abundant protein depletion methods, detection of low-abundant disease-relevant phosphoproteins from complex matrices like biofluids has proven to be difficult [2] . To add to the complexity of analysis, the rapid pace of new bioanalyte discoveries suggests the existence of many presently undiscovered bioanalytes, limiting the advantage of some techniques that require specific knowledge of the analyte properties for separation or detection. In order to obtain useful information from complex samples containing known (targeted) or unknown (untargeted) bioanalytes, sample components must first be effectively partitioned to manageable and measurable numbers.

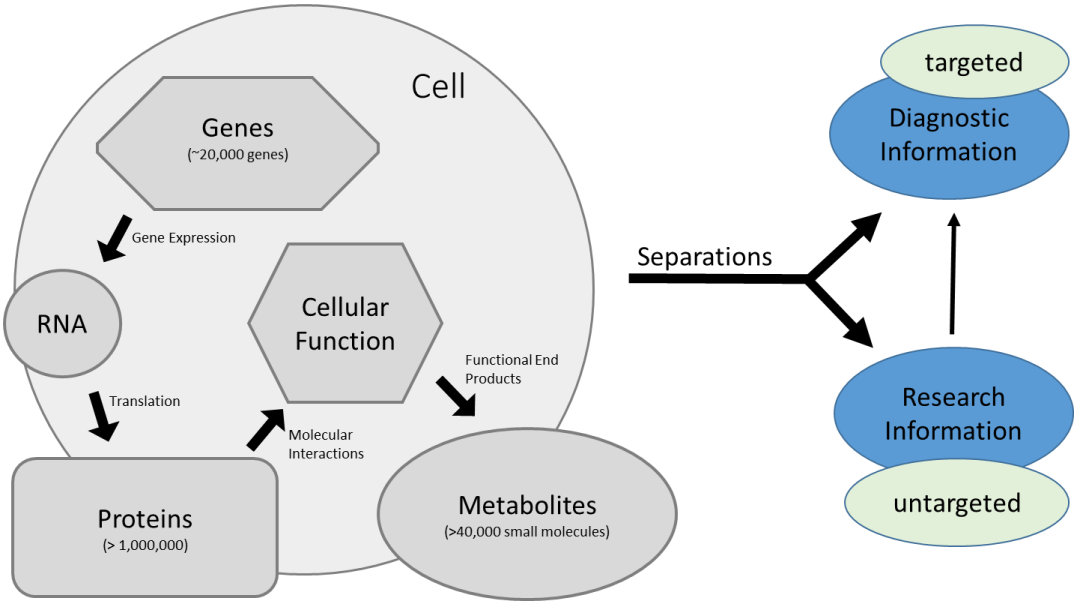

Figure 1.1. Complex separations. Schematic representing the importance of separation science for complex biological sample analysis.

1.2 Separation science

While detection plays an important role in the analytical challenge faced with complex biological samples, the advent of extremely sensitive and dynamic mass spectrometry (MS) detection strategies has largely shifted the analysis bottleneck to a separations problem [3]. Separations is generally defined as the spatial transport and redistribution of the components of mixtures [4-6]. Common examples include filtration, distillation, extraction, centrifugation, chromatography, and electrophoresis. While these partly make up the twenty to thirty core separation techniques from which numerous variations and subcategories often stem, only certain techniques have the characteristics necessary for complex sample separation (Figure 1.2) [4, 5].

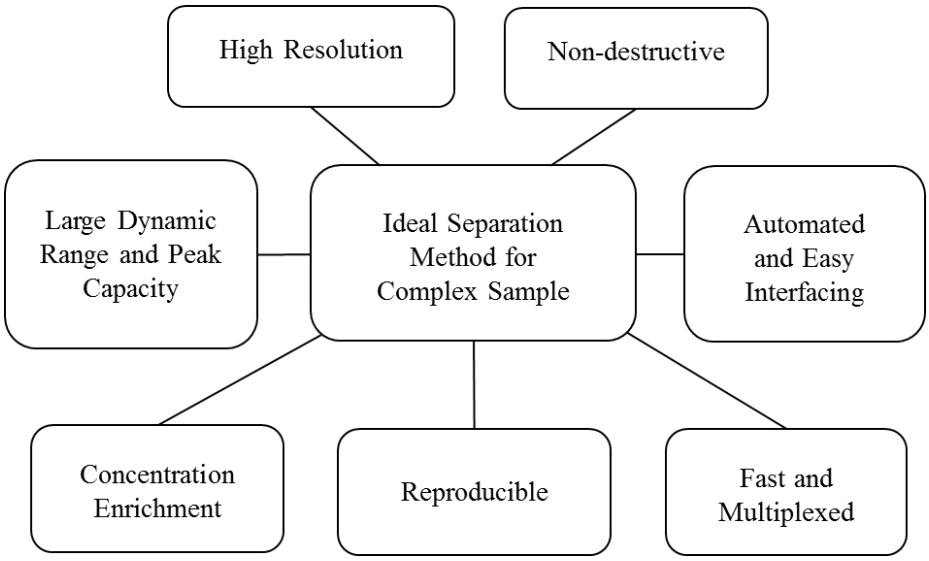

Figure 1.2. Chart outlining key attributes of an ideal separation method for complex samples.

The separation strategies that currently exist for complex samples like bioanalytes often involve the core techniques of liquid chromatography (LC) or electrophoresis (EP) due to their reproducibility, resolution, non-destructiveness, automation and easy interfacing with various detection systems or other separation methods. Although LC-MS has been employed extensively for protein, peptide, and metabolite identification, EP-MS has seen recent growth for disease diagnostics, therapeutic treatment monitoring, and genomic, proteomic, and metabolomic applications as a result of its excellent resolution and the creation of extensive databases made possible by highly reproducible electrophoretic migration profiles [7, 8]. For instance, EP-MS is one of the most attractive analytical methodologies for forensic cocaine metabolite analysis despite previously published methods utilizing immunoassays, GC-MS, and HPLC-MS [9]. Electrophoretic separations can provide excellent separation resolution, compatibility with essentially all buffers and analytes, low liquid consumption, fast analysis,

compatibility with different detection systems, and integration into other separation systems making it a powerful multidimensional option for complex separations [1, 10].

1.3 Capillary electrophoresis

Capillary electrophoresis (CE) has been demonstrated as a high resolution EP separation technique for proteins, peptides, metabolites, DNA, and cells [11-15]. The ability to adjust buffer pH and impart ionic charges, *q*, on analytes residing at physiological pH offers a non-destructive (non-binding) method of separating materials based on their charge to frictional force ratios (or electrophoretic mobility, μ_{ep}), as shown by equation 1.1, where *r* is the ionic radius of the substance and η the buffer viscosity.

$$\mu_{ep} = \frac{q}{6\pi\eta r} \tag{1.1}$$

The high surface to volume ratio offered by the microfluidic dimensions of the capillaries permits application of high voltage, *V*, across the channel length, *L*, to create an electric field, *E*, without generating compromising joule heating. However, working at this scale comes with a cost of limited sensitivity due to small inner diameter capillaries resulting in reduced injection volumes and decreased path length for UV and visible spectroscopic detection.

$$E = \frac{V}{L} \tag{1.2}$$

Within the applied electric field, an injected sample plug comprised of charged analytes with distinct electrophoretic mobilities will begin to separate over time and space as each analyte migrates through the channel with a distinct electrophoretic velocity, v_{ep} (Figure 1.3).

$$v_{ep} = \mu_{ep} * E \tag{1.3}$$

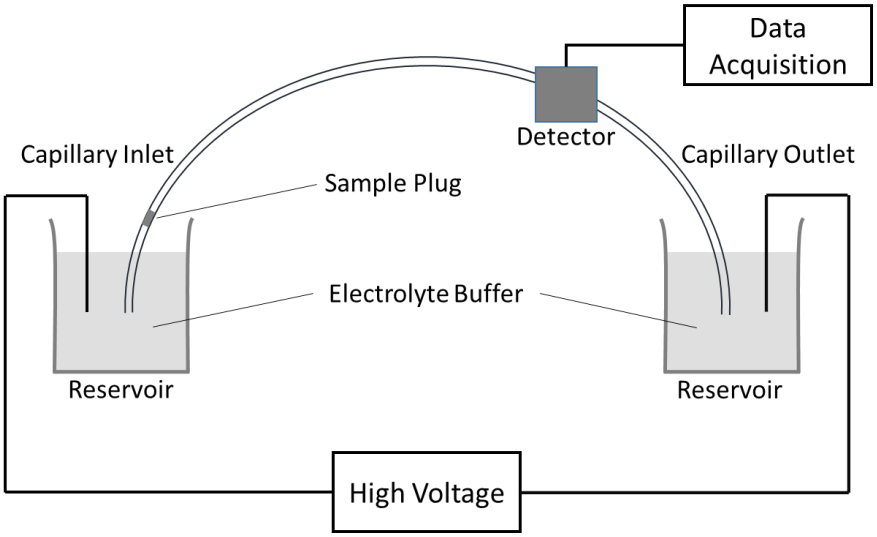

Figure 1.3. Capillary electrophoresis (CE). Basic setup of a CE instrument. Sample plug separates into individual components along capillary length in the presence of an electric field. Electric field is induced by a high voltage power supply and separation is observed using an inline detector.

1.4 Electroosmotic flow

In capillary electrophoresis and other microfluidic EP separations where charged analytes migrate with some velocity in an electric field, bulk fluid movement known as electro-osmotic flow (EOF) must also be considered. EOF occurs when counter ions within the bulk fluid stack against the surface charges residing at a channel wall. In the presence of an electric field, a slip condition results and the counter ions migrate towards the oppositely charged electrode, dragging the remaining bulk fluid in the same direction (Figure 1.4). EOF magnitude is dependent upon the strength of the electric field, viscosity of the bulk fluid, dielectric constant of the bulk fluid, ε, and zeta potential, ζ, that results at the plane of shear close to the liquid-solid interface.

$$\nu_{eo} = \frac{\epsilon\zeta}{4\pi\eta} E \tag{1.4}$$

Because the bulk fluid is driven without an externally applied pressure, the profile of EOF velocity, ν_{eo}, is uniform across the entire channel diameter except very close to the wall where the velocity approaches zero (dashed line in Figure 1.4).

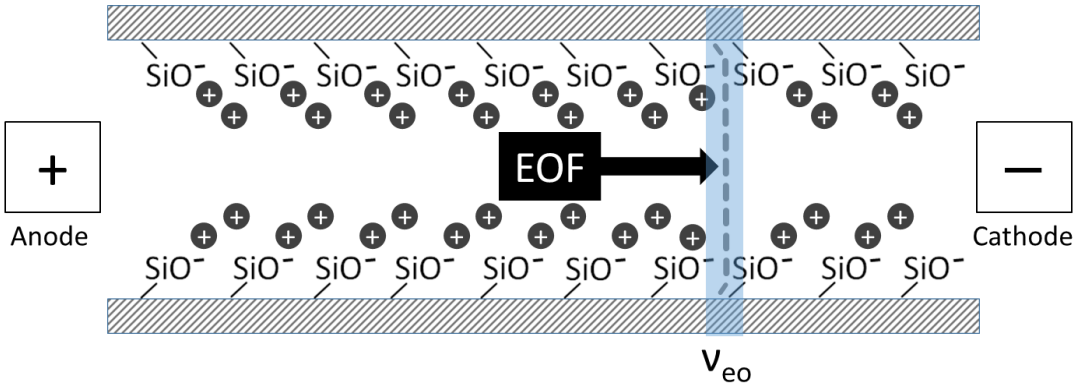

Figure 1.4. Electro-osmotic flow (EOF). Positively charged ions orient next to negatively charged (deprotonated) silanol groups at the channel surface. Dashed line represents flat EOF velocity (ν_{eo}) profile.

1.5 Laminar flow

Externally applied pressure can also be used to drive bulk fluid flow in microfluidic separations applications. In a pressure-driven system, the bulk fluid contains an inertial component that is dependent on velocity, ν, and channel length, L. When the ratio of the fluid inertia to fluid viscosity, known as the Reynolds number, *Re*, is below a threshold of 2000, the frictional forces along the fluid-wall interface cause a parabolic cross-sectional flow profile referred to as laminar flow (Figure 1.5).

$$Re = \frac{\nu L}{\eta} \tag{1.5}$$

Under laminar flow conditions, a considerable velocity gradient exists across the lateral width of the channel compared to the flatter EOF profile. The velocity along the

longitudinal length of the channel reaches a constant maximum approximately one capillary diameter's length inside the channel entrance.

The effective fluid velocity, v_{eff}, (sometimes referred to average fluid velocity) of the laminar profile is dependent upon the pressure change, ΔP, and total hydrodynamic resistance within the channel system. Pressure is often applied using an external pump, vacuum, a gas source, or hydrostatically. With hydrostatic pressure, ΔP is the product of fluid density, acceleration of gravity, and height difference between fluid levels, or $\rho g \Delta h$, respectively. The total hydrodynamic resistance is dependent upon the fluid viscosity and the shape (e.g. cylindrical, rectangular, etc.) and length of the channel system. For a cylindrical pipe like a capillary, the effective velocity can be calculated with Poiseuille's equation (equation 1.6), where the maximum velocity, v_{max}, residing at the center laminae is double the effective velocity (Figure 1.5).

$$v_{eff} = \frac{r^2 \Delta P}{8 \eta L} \text{ (for a cylinder)} \quad (1.6)$$

$$v_{max} = 2 * v_{eff} \quad (1.7)$$

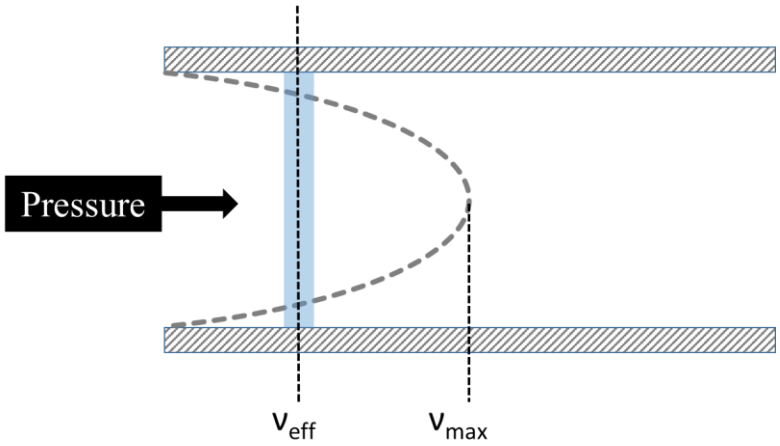

Figure 1.5. Laminar flow. Depiction of a laminar flow profile in a cylinder. Magnitude of the effective velocity (v_{eff}) is one-half that of the maximum velocity (v_{max}) which resides along the channel center.

1.6 Equilibrium gradient focusing

The equilibrium gradient principle summarized by Giddings offers a separations technique that largely overcomes the sensitivity limitation of traditional microfluidic EP separations methods while retaining the high resolution benefit associated with these techniques [16]. Unlike CE, where the analyte zones continuously migrate through the separation domain, equilibrium gradient focusing sets a condition where analyte zones migrate from all parts of the separation domain to a single point of stasis. Separation and concentration occur simultaneously and diffusional band-broadening is minimized as restoring forces on both sides of the equilibrium position act to keep the concentration zone focused.

Equilibrium gradient focusing techniques can be divided into two general categories, both of which employ an electric field to drive charged analytes to a unique and specific position of net zero force [17, 18]. Isoelectric focusing (IEF) is widely regarded as the first of these categories, inducing separation by electrophoretically driving ampholytic analytes (typically proteins or peptides) through a pH gradient using electric field until they reach their distinct isoelectric points and become immobile [19]. The other category, sometimes referred to as counter-flow gradient focusing, employs a force opposite a gradient force to establish the equilibrium condition (Figure 1.6) [20]. In O'Farrell's counteracting chromatographic electrophoresis (CACE) approach, a constant electrophoretic velocity was opposed to a gradient hydrodynamic velocity induced by varying chromatographic matrices within a separation column [21]. Other counter-flow gradient focusing techniques that followed utilized a hydrodynamic velocity opposed to a gradient electrophoretic velocity induced by establishing conductivity [22], electric field

[23-26], or temperature [27, 28] gradients within the system. Both equilibrium gradient focusing techniques allow simultaneous separation and concentration enhancement over time, but unlike IEF which requires ampholytic samples, counter-flow gradient focusing can be applied to virtually any electrophoretically mobile substance.

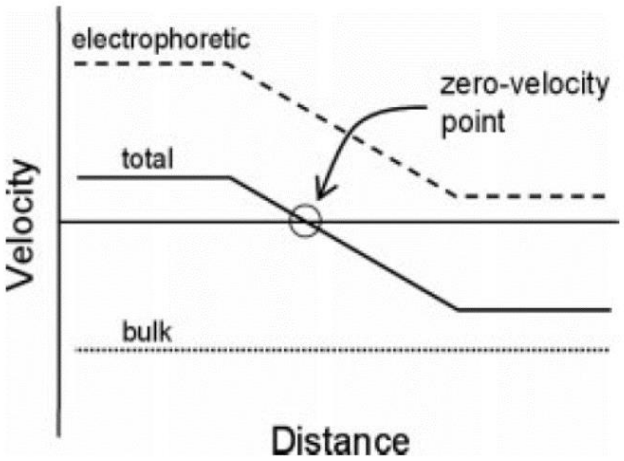

Figure 1.6. Counter-flow gradient focusing. Here, a constant bulk fluid velocity counters a gradient electrophoretic velocity establishing a net zero velocity point [20].

1.7 Electrophoretic exclusion

Electrophoretic exclusion is a form of counter-flow gradient focusing where charged analytes can be excluded from entering a channel by countering hydrodynamic velocity with electrophoretic velocity at the entrance interface (Figure 1.7) [29, 30]. While most other counter-flow gradient focusing techniques establish a smooth varying or incrementally stepped gradient within the confines of a channel to serially separate and concentrate analytes, electrophoretic exclusion establishes a single, distinct interfacial exclusion zone at the channel entrance in an attempt to generate high fidelity differential transport to allow very similar species to be separated at the interface [31].

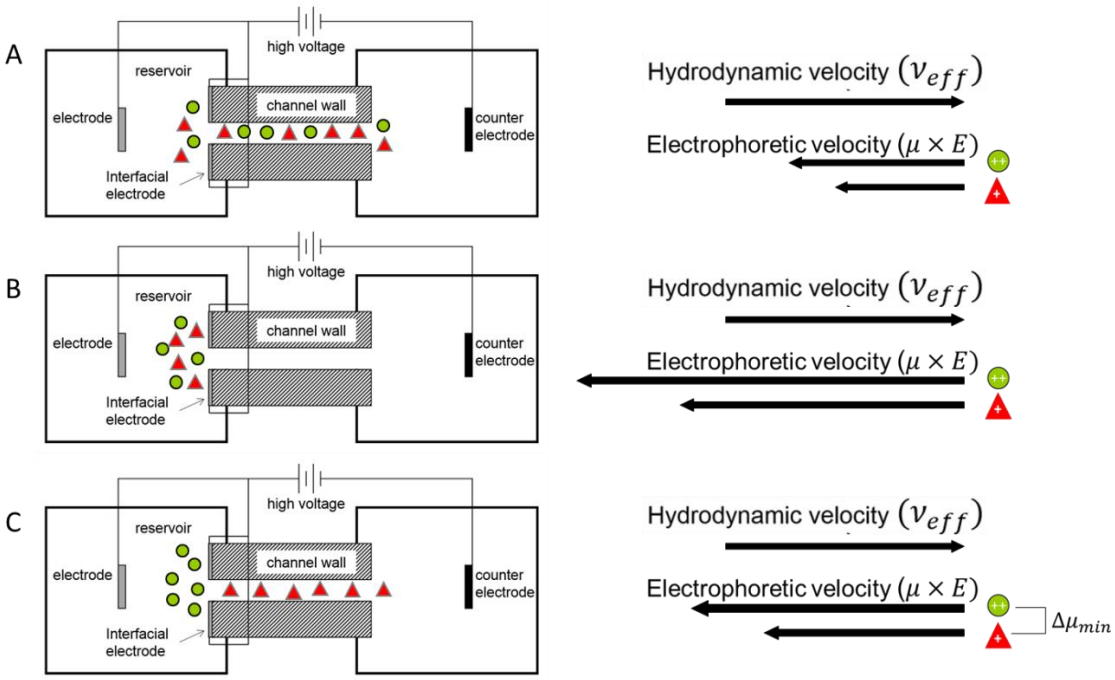

Figure 1.7. Principle of electrophoretic exclusion. Green circles represent cations with a higher electrophoretic mobility (μ) than the orange triangle cations. Electric field (E) is established in the channel by the high voltage supply. (A) No exclusion; both analytes enter the channel and flow to the exit reservoir (right side). (B) Full exclusion; neither analyte enters the channel. (C) Differential exclusion; the green circle cations are excluded but the orange triangle cations enter the channel and flow to the exit. The minimum μ difference between two analytes that can still be separated at the interface is represented by $\Delta\mu_{min}$.

In its simplest form as a single-channel separation interface, electrophoretic exclusion has limited separation capability for complex samples since all analytes will either enter the channel or be excluded. However, unique separation capabilities emerge when considering the coupling of multiple channel entrances in series and in parallel (Figure 1.8). Coupled interfaces provide punctuated microgradient separation zones and the opportunity to adjust each interfacial exclusion threshold independently allowing for a multiplexed separation array similar to immunoassay arrays. A significant difference, however, is that coupled interfaces allow for customizable separation parameters that could easily be changed on the fly to target specific analytes with known electrophoretic

mobilities or as a screening method for an untargeted approach (Figure 1.8, C). This arrangement offers the flexibility to concentrate very dilute analytes to the linear range of detection while simultaneously removing unwanted or interfering components from the separation domain. A feature like this is typically not achievable with traditional single channel linear separations like liquid chromatography, gas chromatography, or capillary electrophoresis where the entire separation domain is dependent on a single set of global separation parameters. Furthermore, follow-on analysis of specific analytes of interest captured in independent exclusion reservoirs could be accomplished without having to elute the entire separation domain like in traditional linear methods, helping to minimize band broadening and the necessity for an additional fractionation strategy to collect the analytes of interest. The principle of electrophoretic exclusion as a way to segregate, enrich, and access targeted and untargeted analytes, or group of analytes based on their closely related properties, warrants further exploration into this potentially powerful separation strategy.

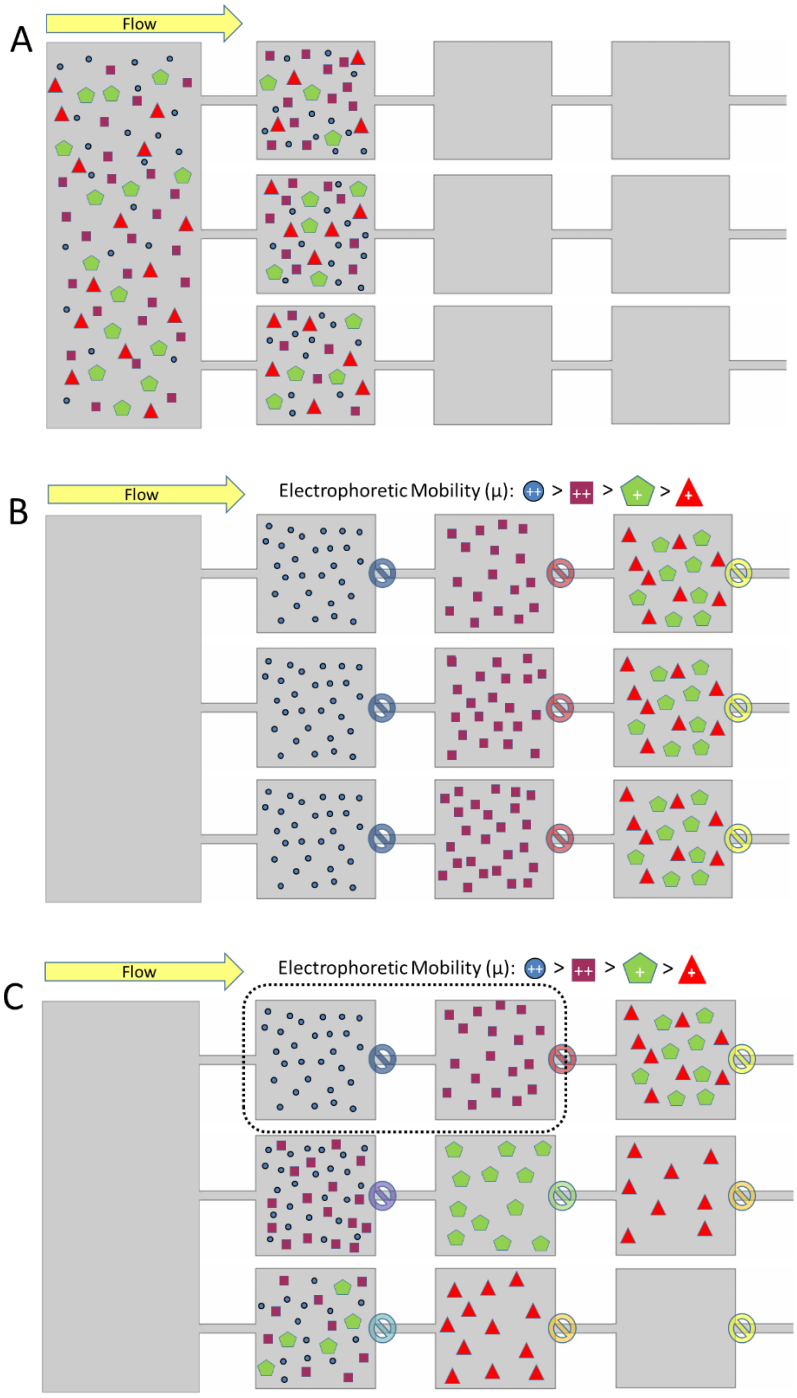

Figure 1.8. Electrophoretic exclusion in a simple array format. The outlined region in C represents a single interface as shown in Figure 1.7. (A) Mixture of four analytes flow from a bulk reservoir to exclusion reservoirs connected in parallel. Applied electric field creates exclusion parameters (Ø) at each interface in (B) and (C). Exclusion parameters between parallel interfaces in (B) are the same (indicated by like colors), demonstrating multiplexed enriching capability. Exclusion parameters between each interface in (C) vary, demonstrating multiplexed separation capability.

1.8 Dissertation objectives

The focus of this dissertation is the advancement of the separations technique termed electrophoretic exclusion. Initial objectives included the preliminary design and fabrication of a benchtop device to demonstrate small molecule exclusion and concentration enhancement. The remainder of the work focused on a fundamental investigation of the flow velocities, electric fields, and molecular transport near the channel entrance where exclusion occurs to better understand the features that directly impact the quality of separation.

1.9 Dissertation summary

The capability of excluding molecules at a single channel interface is necessary before combining multiple interfaces in series and in parallel to meet the high throughput demands of complex samples. Initial design and fabrication of a capillary-based electrophoretic exclusion device with interfacial electrode are detailed in Chapter 2. Additionally, results demonstrating successful capture and simultaneous concentration of methyl violet within the proximity of the entrance are presented. Electrophoretic exclusion offers the unique possibility of simultaneous separation and concentration in bulk solution but relies heavily on the velocity and electric fields at the channel entrance warranting further investigation into this region.

The interfacial region where exclusion occurs is characterized by quantifying the center laminae velocity and electric field magnitudes using particle tracking velocimetry (Chapter 3). The suspected lateral gradient field effects near the entrance corners, as suggested in Chapter 3, is explored using fluorescent microscopy and inline spectroscopy with rhodamine 123 (Chapter 4). Both studies include finite element models that

quantitatively (Chapter 3) and qualitatively (Chapter 4) agree with the detailed results giving credibility to the models and their use to drive design modifications. These studies provide insight into the longitudinal and lateral gradient effects that add complexity to the exclusion interface.

The foundational framework of the recently described electrophoretic exclusion resolution theory is built upon by first experimentally assessing the current device resolving capability using rhodamine 6G and rhodamine B (Chapter 5). A method is then developed to assess resolution within the simulations to allow the model to be compared to the experimental results and theoretical predictions. Resolution assessment using the simulation also affords direct comparison of different model designs so as to have a metric for evaluating design performance. Consistency is demonstrated between the simulation and experiment resolution results and general agreement exists with the theoretical equation predictions providing a proof-of-concept for using the model construct as a tool to quickly assess resolution for optimizing performance of varying device designs.

1.10 References

[1] Kler, P. A., Sydes, D., Huhn, C. *Anal. Bioanal. Chem.* 2015, *407*, 119-138.

[2] Iliuk, A. B., Arrington, J. V., Tao, W. A. *Electrophoresis* 2014, *35*, 3430-3440.

[3] El-Baba, T. J., Lutomski, C. A., Wang, B., Inutan, E. D., Trimpin, S. *Anal. Bioanal. Chem.* 2014, *406*, 4053-4061.

[4] Giddings, J. C. *Unified separation science*, New York, Wiley 1991.

[5] Karger, B. L., Snyder, L. R., Horváth, C. *An introduction to separation science*, New York, Wiley 1973.

[6] Macášek, F., Navratil, J. D. *Separation chemistry*, New York, Ellis Horwood 1992.

[7] Zhao, S. S., Zhong, X., Tie, C., Chen, D. D. Y. *Proteomics* 2012, *12*, 2991-3012.

[8] Albalat, A., Mischak, H., Mullen, W. *Expert Review of Proteomics* 2011, *8*, 615-629.

[9] Rodriguez Robledo, V., Smyth, W. F. *Electrophoresis* 2014, *35*, 2292-2308.

[10] Kolch, W., Neusüß, C., Pelzing, M., Mischak, H. *Mass Spectrom. Rev.* 2005, *24*, 959-977.

[11] Jorgenson, J., Lukacs, K. *Science* 1983, *222*, 266-272.

[12] Issaq, H. *Electrophoresis* 1999, *20*, 3190-3202.

[13] Jorgenson, J., Lukacs, K. *J. Chromatogr.* 1981, *218*, 209-216.

[14] Jorgenson, J., Lukacs, K. *Anal. Chem.* 1981, *53*, 1298-1302.

[15] Kuehnbaum, N. L., Britz-McKibbin, P. *Chem. Rev.* 2013, *113*, 2437-2468.

[16] Giddings, J. C., Dahlgren, K. *Separation Science* 1971, *6*, 345-356.

[17] Wang, Q., Tolley, H., LeFebre, D., Lee, M. *Anal. Bioanal. Chem.* 2002, *373*, 125-135.

[18] Ista, L., Lopez, G., Ivory, C., Ortiz, M. *et al*. *Lab on a Chip* 2003, *3*, 266-272.

[19] Righetti, P. G., Drysdale, J. W. *Isoelectric focusing*, Amsterdam, North-Holland Pub. Co. 1976.

[20] Shackman, J. G., Ross, D. *Electrophoresis* 2007, *28*, 556-571.

[21] Ofarrell, P. H. *Science* 1985, *227*, 1586-1589.

[22] Greenlee, R. D., Ivory, C. F. *Biotechnol. Prog.* 1998, *14*, 300-309.

[23] Koegler, W. S., Ivory, C. F. *Biotechnol. Prog.* 1996, *12*, 822-836.

[24] Koegler, W. S., Ivory, C. F. *Journal of Chromatography a* 1996, *726*, 229-236.

[25] Huang, Z., Ivory, C. F. *Anal. Chem.* 1999, *71*, 1628-1632.

[26] Astorga-Wells, J. *Anal. Chem. (Wash.)* 2003, *75*, 5207-5212.

[27] Ross, D., Locascio, L. E. *Anal. Chem.* 2002, *74*, 2556-2564.

[28] Shackman, J. G., Munson, M. S., Kan, C., Ross, D. *Electrophoresis* 2006, *27*, 3420-3427.

[29] Hori, A., Matsumoto, T., Nimura, Y., Ikedo, M. *et al*. *Anal. Chem.* 1993, *65*, 2882-2886.

[30] Polson, N. A., Savin, D. P., Hayes, M. A. *J. Microcolumn Sep.* 2000, *12*, 98-106.

[31] Pacheco, J. R., Chen, K. P., Hayes, M. A. *Electrophoresis* 2007, *28*, 1027-1035.

Chapter 2

Concentration of small molecules using electrophoretic exclusion

2.1 Introduction

The field of separations science plays an important role in the analysis of complex biological samples, often requiring high resolution, high throughput, multidimensional separation strategies. While chromatographic strategies are heavily relied upon for these types of analyses, their inherent problems with protein dispersion, poor compatibility with detergents, and low recovery of certain proteins has resulted in a renewed interest in electrophoretic separations [33]. The utilization of electric fields as a separation mechanism offers multiple advantages: (i) quantitative information derived from distinct migration times [34, 35]; (ii) simple and cost effective integration into parallel microfluidic systems; (iii) easily adjustable separation fields allowing for numerous programmable configurations; (iv) the option to separate other surface-charged species of interest such as microbes or cells .

Capillary and microchip electrophoresis are two such electrophoretic separation techniques that have been used extensively with biological samples [5-11]. Despite these advantages and numerous applications, capillary and microchannel electrophoresis systems most commonly suffer from limited sensitivity [12, 13]. To overcome the sensitivity issue, several pre-concentration methods have been investigated and reviewed at length [14-21]. Common examples include field-amplified sample stacking [22], isotachophoretic stacking [23, 24], and dynamic pH junction [25, 26], among others. Another approach, sometimes referred to as ‘counter-current electro-concentration’ [15] or ‘counter-flow gradient focusing’ [21, 27], relies on the ‘equilibrium gradient’ approach

where an imbalance of force exerted on an analyte within a separation domain causes it to move to a position of zero net force, allowing simultaneous separation and concentration and reduced band broadening [28]. Counter-flow gradient focusing establishes the equilibrium condition by countering an electrophoretic force with bulk solution flow resulting in charged analytes coming to rest where their electrophoretic velocities equal the counter-flow [27].

The technique used for the current work is termed 'electrophoretic exclusion' and encompasses counter-flow gradient focusing at the entrance of a channel by countering electrophoretic velocity with hydrodynamic velocity. Although several techniques have been explored to establish a counter-flow gradient condition, the separation zone has predominantly been within the confines of a channel where longitudinal flow and electric fields are fully developed and at their maxima along the respective longitudinal laminae, thereby necessitating the intentional establishment of a longitudinal separation gradient using chromatographic beds, tapered geometry, temperature changes, electrode arrays, or other means [29-35]. Hori *et al.* explored using the naturally occurring longitudinal electric field and fluid velocity gradients at a converging channel entrance to create a counter-flow gradient separation zone [36]. Results demonstrated modest concentration enhancement of herring DNA and 2,6-naphthalenedisulfonic acid, but the large volumes and 1.5 mm large-bore channels limited large concentration enhancement and introduced some stability issues with the electric currents and pressure. A similar configuration by Polson *et al*. utilized 20 μm inner diameter channels and an electrode fabricated at the entrance to demonstrate the exclusion and concentration enhancement of 200 nm carboxylate modified latex spheres within the immediate volume of the channel entrance

[37]. Pacheco *et al.* further developed the electrophoretic exclusion construct by establishing the centerline threshold value required to achieve a focusing condition at a converging reservoir-to-channel entrance. [38].

Work presented in this chapter uses a flow injection technique to evaluate electrophoretic exclusion of small molecules. Methyl violet, a cationic dye, with visible spectroscopy detection were used to monitor flow and electrophoretic dynamics to demonstrate and characterize device functionality. The capability of excluding molecules at a single channel interface is necessary before combining multiple interfaces in series and in parallel to meet the high throughput demands of complex samples. The successful capture and simultaneous enrichment of methyl violet at the channel interface region was demonstrated.

2.2 Materials and methods

2.2.1 Reagents

The bulk fluid buffer was comprised of sodium phosphate (Sigma Aldrich, St. Louis, USA) and 18 MΩ water at pH 2.85 and 25 mM. Methyl violet 2B (Sigma Aldrich, St. Louis, MO) with $\mu_{ep} = 1.7 \times 10^{-4}$ $cm^2V^{-1}s^{-1}$ (determined experimentally using CZE) was prepared at 5 µM in the phosphate buffer and chosen as the analyte for the preliminary spectroscopy studies do to its visible detection and positive charge at low pH. Concentrated hydrochloric acid (HCl, EMD, Savannah, GA) was diluted to 0.1M with 18 MΩ water.

2.2.2 Device fabrication

The electrophoretic exclusion device was fabricated in house by connecting two reservoirs with a channel that had an electrode placed exactly at the entrance reservoir-channel interface (Figure 2.1). The reservoirs consisted of 2 mL glass vials connected with a 14 cm polyimide-coated fused silica capillary (75 μm i.d./ 365 μm o.d., Polymicro Technologies, Phoenix, AZ)) mounted on a rotatable board to control hydrostatic pressure difference between fluid levels. Construction of an interfacial electrode was accomplished by removing approximately 3 mm of polyimide coating from the cleaved capillary end and sputter coating it with a 30 nm layer of titanium then 50 nm platinum [39]. Care was taken to maintain a flat capillary face during cleaving to avoid undesirable electric and flow field variations that may occur if sharp, irregular geometric features exist at the interface. To electrically connect the sputtered face, silver conducting epoxy was applied to the side of the sputtered tip and to a platinum wire that extended into the entrance reservoir while connected to a CZE1000R high voltage power supply (Spellman High Voltage Electronics Corporation, Hauppauge, NY) (Figure 2.1, far left image). All conducting areas except the capillary face and electrode extending into the reservoir were coated with clear epoxy to render them electrically nonconductive and nonreactive in solution. The opposite, non-sputtered capillary end was epoxied into a separate glass vial along with a platinum wire placed in the bulk buffer solution and not electrically connected to the tip. Each wire was connected to opposite terminals of the high voltage

power supply to complete the circuit when buffer was present (Figure 2.1, B).

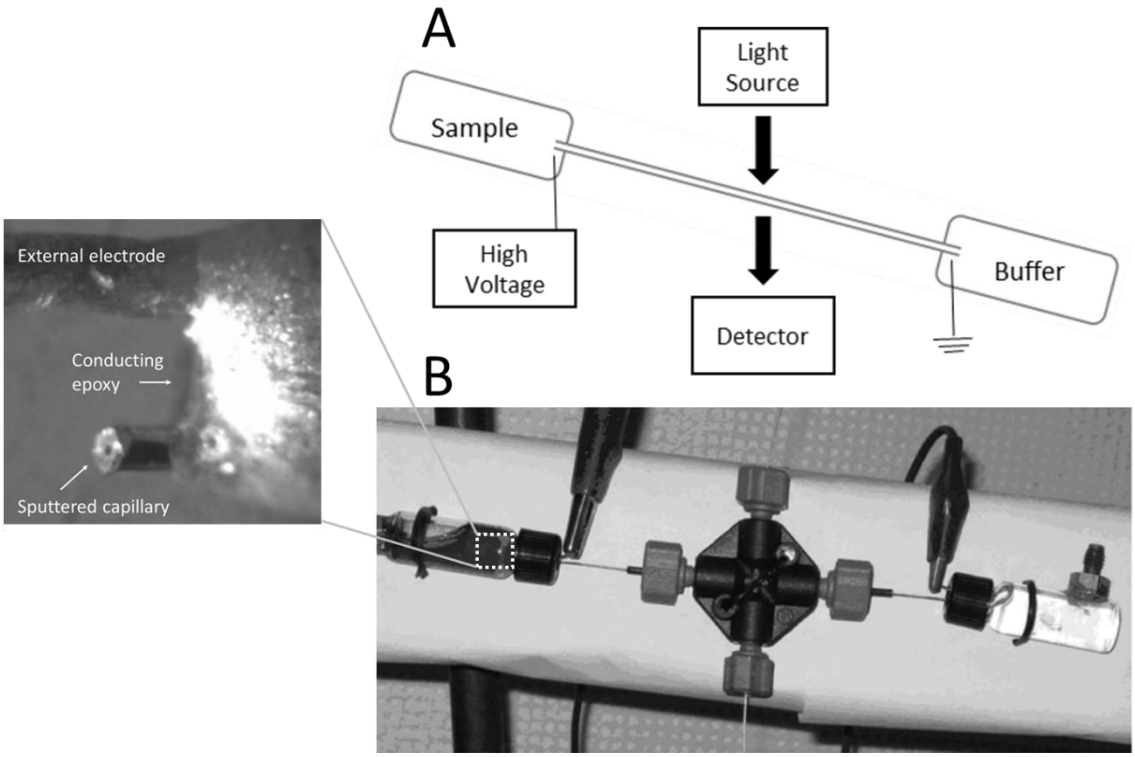

Figure 2.1. Initial exclusion device. Setup of flow injection analysis of an electrophoretic exclusion device [39]. (A) Sample and buffer reservoirs connected by a channel with integrated fiber optic visible spectroscopy detection. High voltage across the channel establishes electric field; height difference between reservoirs establishes hydrostatic pressure for fluid flow. (B) Actual experimental setup as in (A) showing zoomed image of the interfacial electrode configuration (far left) and alligator clips connecting electrodes to the high voltage supply.

Detection using visible spectroscopy was incorporated inline approximately midway between the capillary entrance and exit using a fiber optic-based spectrometer comprised of a Mikropack DH-2000 UV-vis light source, CUV CCE Electrophoresis sample cell, a USB2000 Spectrometer, and OOIBase software (all Ocean Optics, Dunedin, FL). A 580 nm absorbance wavelength was monitored for the methyl violet channel and a 675 nm wavelength was monitored as a control.

2.2.3 Experimental parameters

Prior to all experiment trials, the system was preconditioned with 0.1 M HCl for no less than 10 minutes, followed by a minimum 5 minute rinse of the separation buffer at pH 2.85. The fluid meniscus heights within the reservoirs were offset between 1.0 cm and 4.5 cm over different trials equating to a net positive hydrodynamic velocity (from channel entrance to exit) ranging from 123 µm/s to 552 µm/s. Applied potentials were approximately 1 kV, monitored by the power supply analog indicator.

2.3 Results and discussion

2.3.1 Principles of electrophoretic exclusion

Electrophoretic exclusion is achieved when the electrophoretic velocity of a substance in an applied electric field is equal to or greater than the bulk fluid velocity moving in the opposite direction. Equation 2.1 is an adaptation of the dimensionless parameter *S* from Pacheco *et al*. that represents the ratio of electrophoretic velocity to fluid velocity [38]. When S ≥ 1 for a particular species, the electrophoretic exclusion condition is satisfied and entrance of that species into the channel is not expected. All variables have been previously defined in Chapter 1, (equations 1.1, 1.2, and 1.6).

$$S = \frac{v_{ep}}{v_{eff}} = \frac{\mu_{ep} E}{v_{eff}} = \frac{\frac{q}{6\pi\eta r_{ionic}}\left(\frac{V}{L}\right)}{\frac{r^2 \Delta P}{8\eta L}} = \frac{4qV}{3\pi r_{ionic} r^2 \Delta P} \tag{2.1}$$

A noteworthy absence from equation 2.1 is an EOF term that is generally part of electrophoretic systems. To simplify the control and assessment of the electrokinetic effects during the preliminary characterization stages of electrophoretic exclusion, it was assumed that EOF effects were minimized by treating the inner surfaces of the capillary and reservoirs to limit surface charges. This study maintained the buffer pH below the

ionizing pK_a of the silanol groups located on the surface of the channel and reservoir walls to minimize EOF effects [40].

The experimental parameters found in equation 2.1 can be adjusted to achieve the electrophoretic exclusion condition. Although maximizing both the analyte charge and applied voltage (to increase v_{ep}) while minimizing the channel radius and applied pressure (to decrease v_{eff}) contribute to achieving a maximum exclusion threshold, consideration was given to the goals and tradeoffs during experimental design. For instance, minimizing channel radius and applied pressure reduced the hydrodynamic velocity enabling a lower voltage requirement and lessening the chance of undesirable electrochemical effects, but this came at the cost of slowing the rate of enrichment during exclusion. Another consideration was that of analyte charge, q. Exclusion at pH 2.85 helped control EOF, but the number and type of biological components that carry a net ionic charge at this pH was limited compared to buffer conditions near physiological pH. To maximize the number and type of biological components that can be effectively separated with this technique, coated channels or other means to control EOF can be used [41]. Adjustment of the channel length, L, and buffer viscosity (equations 1.1, 1.2, and 1.6) have little to no overall effect on the established exclusion threshold, however, since both parameters equally affect the countering velocity vectors as shown in equation 2.1. Particular attention must therefore be given to the applied voltage, hydrostatic pressure, channel width, and buffer composition in context with the desired rate of concentration enhancement and analyte composition when designing a device to maximize the condition for electrophoretic exclusion.

2.3.2 Concentration enhancement of cationic molecules

Flow injection analysis provided a method to assess the exclusion dynamics of the experimental system. This method of analysis incorporated a detection zone midway down the channel to assess concentration variations over time before, during, and after the exclusion process. With known hydrodynamic velocity, distance from entrance to detector, and timing of all events, the original location of any concentration enrichment zone reaching the detector could be back-calculated. Methyl violet was added to the entrance reservoir, and flow through the channel was observed and verified by monitoring the increased absorbance signal as methyl violet entered the detection zone approximately midway down the channel (Figure 2.2). Hydrodynamic velocity within the channel was determined theoretically using hydrostatic pressure and Poiseuille's equation (equation 1.6) and experimentally by measuring the time for the methyl violet to reach the detection zone after being injected 7.5 cm upstream. The 7% relative standard error between the calculated velocity and experimental velocity measurements indicated that flow injection analysis was a feasible, albeit indirect, method for generally assessing the electrophoretic exclusion performance.

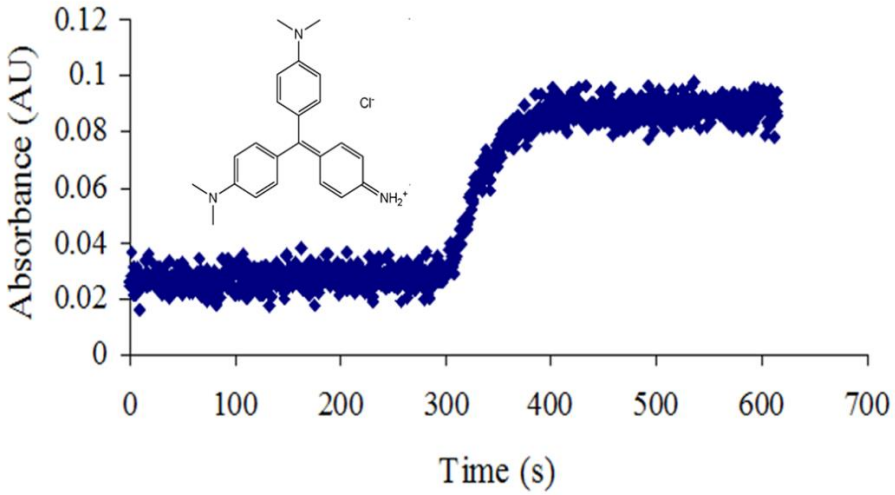

Figure 2.2. Flow injection analysis. Absorbance plot showing introduction of methyl violet into the electrophoretic exclusion instrument. Absorbance from 0-300 seconds is buffer only. Absorbance from 300-600 seconds is methyl violet flowing past detector and reaching steady state. Left Inset showing methyl violet structure and resident +1 charge.

After methyl violet concentration reached steady state as indicated by the absorbance signal plateau, varying durations of electric potential were independently applied to the cathode residing at the channel interface reservoir. Upon removal of the applied potential, the absorbance signal was monitored for a duration no less than the calculated time required for the buffer at the channel entrance to reach the detection zone (136 s in this case). Figure 2.3 is a compilation of the methyl peaks resulting from the various durations of applied potential. A rise in methyl violet concentration occurred in 6 different trials where a 1 kV potential was applied for a duration of 10 seconds up to a maximum duration of 450 seconds while monitoring the absorbance of methyl violet. Interestingly, the full exclusion condition as calculated by equation 2.1 was not necessary for concentration enhancement during these preliminary trials, but subsequent experiments demonstrated similar peak profiles at theoretical full exclusion [39]. The

average time across all trials for the peaks to arrive at the detector after the removal of the electric field was 146 ± 10 s, correlating with the calculated 136 s entrance-to-detector flow injection time and supporting the electrophoretic exclusion principle that predicts the zone of increased methyl violet concentration will occur within the vicinity of the channel entrance.

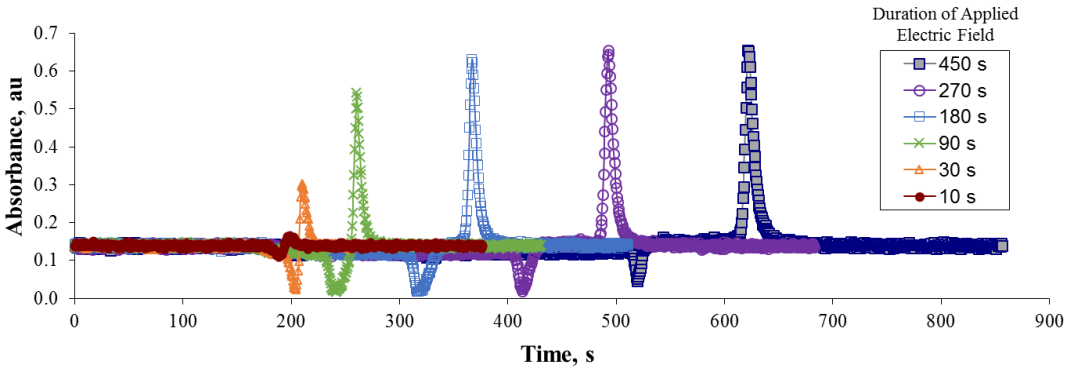

Figure 2.3. Methyl violet exclusion. Compilation of methyl violet absorbance spectra obtained by applying an electric field across the channel over varying durations.

Data also suggested a direct correlation between the duration of the applied electric field and the concentration enhancement of methyl violet, represented by the increasing peak areas in Figure 2.4. The plot of the potential duration versus methyl violet peak areas resembled an error function, consistent with the prediction that dispersive forces (diffusion and convection) will exist within a steady state system containing concentration enrichment zones and hydrodynamic flows. While the electrophoretic exclusion model predicts restorative forces on both sides of the equilibrium position to minimize dispersion, the flattening of the absorbance plot between 270 s and 450 s indicated increased influence of dispersive forces. This may be attributed to the concentration band extending beyond the localized equilibrium position located slightly within the channel and into the open reservoir where dispersive forces

dominate. In a separate study, Meighan *et al*. employed a micro stir bar near the channel entrance to exaggerate dispersion resulting in no discernable concentration buildup despite having met the previously established exclusion threshold [39]. In this case, concentration enhancement was still expected in the bulk solution of the relatively large sample reservoir, but longer exclusion durations would have been necessary to reach the limit of detection for the flow injection analysis protocol. The data from the present study supported the notion that a barrier for molecular charged species can be established and maintained near the reservoir-channel interface using electrophoretic exclusion and underscored the importance of small volume reservoirs if the objective is bulk concentration monitoring.

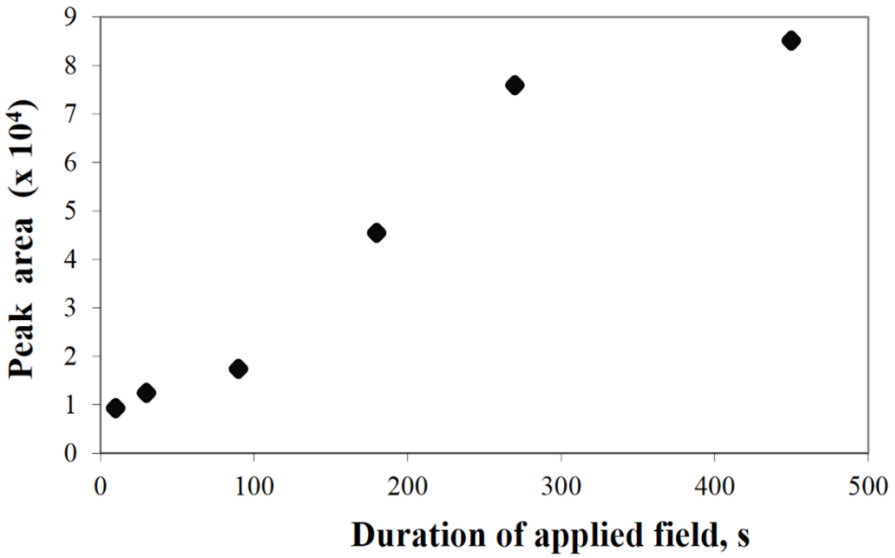

Figure 2.4. Methyl violet concentration enhancement. Methyl Violet peak areas as a function of applied potential duration.

2.3.3 Positive peak assessment

The methyl violet positive peak was used to further assess the in-channel dynamics of the system. A methyl violet peak was created similar to before by applying potential for 120 s, 30 s after the start of the spectroscopic data collection (Figure 2.5,

shaded area I). However, as soon as the concentration band reached the detection zone (indicated by peak b in Figure 2.5), the electric field was immediately regenerated for 120 s (Figure 2.5, shaded area II). Under a full exclusion condition, the band of methyl violet ions in the detection zone would be expected to reverse direction and begin moving towards the entrance when potential was applied (Figure 2.5, shaded area II). However, the position and general appearance of peak *b* (Figure 2.5) inside the channel did not indicate an ion direction change or band broadening, thereby supporting the notion that the full exclusion threshold had not been met despite consistent evidence of concentration enhancement near the entrance.

An assessment of the entrance region dynamics could also be made. Earlier experiments showed that a peak very similar to peak *b* in Figure 2.5 would have been created given the 1 kV potential initiated at 480 s (shaded area II). However, with polarity immediately reversed at 600 s (shaded area III; anode now at entrance), the characteristic shape of the methyl violet peak was affected (Figure 2.5, peak *d*). The peak height was reduced and the band was noticeably wider, both of which would be expected if methyl violet cations collecting near the entrance cathode were suddenly redirected away by the polarity switch. This demonstrated that although a full exclusion threshold may not have existed within the channel, the field near the entrance was strong enough to manipulate the charged species.

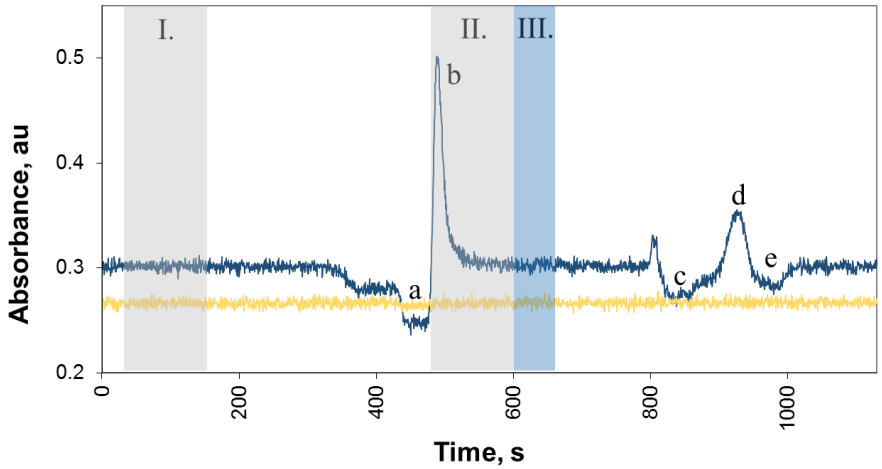

Figure 2.5. Positive peak assessment. Assessment of the system positive and negative peaks. Spectroscopic monitoring occurred at 580 nm (blue plot) and 675 nm (yellow plot) for methyl violet and the control, respectively. A -1 kV potential was applied for 120 s then removed (I). Another -1 kV potential was applied immediately upon arrival of the concentration band (peak b) in the detection window and held for 120 s (II). Polarity was immediately switched (+1 kV) and held for 60 s then removed (III).

2.3.4 Negative peak assessment

A noteworthy negative peak, or dip in absorbance signal, occurred consistently and before every positive peak during the normal exclusion conditions established for these trials (Figure 2.3; Figure 2.5 dip *a*). In each case, the dip did not appear in any of the controls. The total time between the start of the downward absorbance baseline shift and the first appearance of the peak matched the total duration of applied potential. This can be seen in Figure 2.5, where the potential duration of 120 s (shaded area I) is followed by a baseline dip (*a*) starting at 350 s and ending at 470 s, when peak *b* forms. The same observation was made for data in Figure 2.3, though at longer potential durations the initial baseline decrease was less noticeable likely due to methyl violet dispersion back into that region.

An increased distance between dip and methyl violet peak was also apparent with longer potential durations (Figure 2.3). Assuming methyl violet was being collected near the entrance, as already demonstrated, the proximity of the dip relative to the detector at a given time could be calculated. The distance between the dip and detector decreased linearly as the duration of applied field increased (Figure 2.6), indicating a relatively constant velocity of 130 µm/s toward the detector. The fact that the dip velocity towards the detector was less than the calculated hydrodynamic velocity of 552 µm/s but greater than the methyl violet collecting at the entrance suggested this zone had an independent migration towards the entrance.

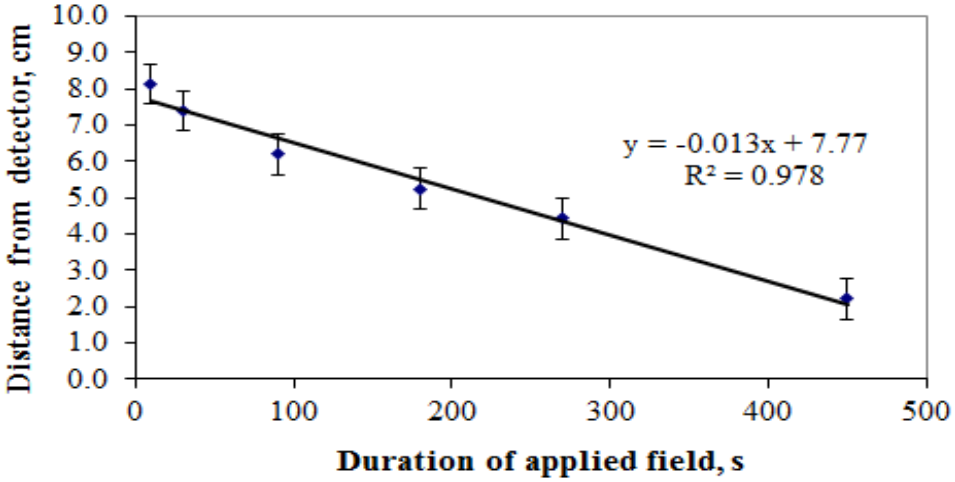

Figure 2.6. Negative peak velocity. Distance between dip and detector calculated using hydrodynamic velocity. The longer the duration of applied potential, the shorter the time it takes for the dip to reach the detector (from Figure 2.3).

While negative peaks, sometimes termed system peaks, are not uncommon in capillary electrophoresis systems, they have often been attributed to the disturbance of a uniform background electrolyte (BGE) by the introduction of zones with compositions different from the BGE, often occurring from sample injections or from co-ion/counter-

ion stacking [42-46]. In this study, positively charged sodium ions and negatively charged phosphate and chloride ions existed along with the methyl violet in solution. Stacking of sodium cations at the entrance was feasible, but they have an electrophoretic mobility more than three times that of methyl violet [45], making it unlikely they would assume a net velocity towards the detector while methyl violet remained at the entrance. The phosphate and chloride anions, on the other hand, would have assumed a net force towards the channel exit with a velocity consisting of both hydrodynamic and electrophoretic velocity components exceeding the observed 130 μm/s. Attributing BGE non-uniformity to the cause of the dip was further evaluated by replacing the phosphate buffer with aspartic acid buffer at its zwitterionic pH of 2.85 to reduce the number of electrokinetic sample components. Despite the presence of only two ionic components - methyl violet and sodium ions - a negative peak was still observed under similar exclusion conditions. These results suggested that something other than injection or co-ion/counter-ion stacking was the primary contributor to the dip.

Another consideration for the negative peak was an induced-charge electro-osmosis (ICEO) effect occurring near the channel entrance resulting from field leakage and local polarization at the sharp corners of dielectric walls [47, 48]. Takhistov *et al*. described vortices arising from mixed pressure-driven and electro-osmotic flow at microchannel junctions with similar electrode and channel configuration as those in the present study (Figure 2.7 A) [49].

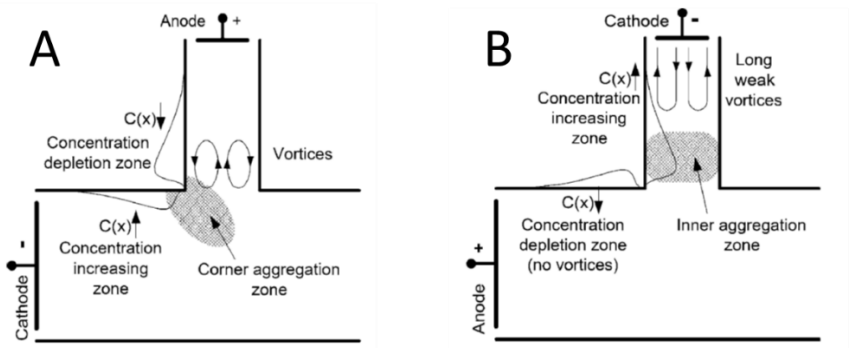

Figure 2.7. Electro-osmotic flow induced vortices in narrow channels for different electrode configurations. (A) Anode resides in the narrow channel and cathode in the larger channel, similar to the configuration used for exclusion in the present study. Takhistov *et al*. [49]. A concentration depletion zone is located just inside the channel with a concentration increasing zone further out towards reservoir. (B) Cathode and anode reversed causing reversed positions of concentration zones.

While it is unclear if a similar ICEO effect would occur at a capillary face with interfacial electrode, reversing the polarity during electrophoretic exclusion consistently resulted in reversal of the positive peak and negative dip positions (Figure 2.5, dip *e*; Figure 2.8), showing characteristics generally similar to those found in comparable device configurations where vortices can form near the entrance corners (Figure 2.7).

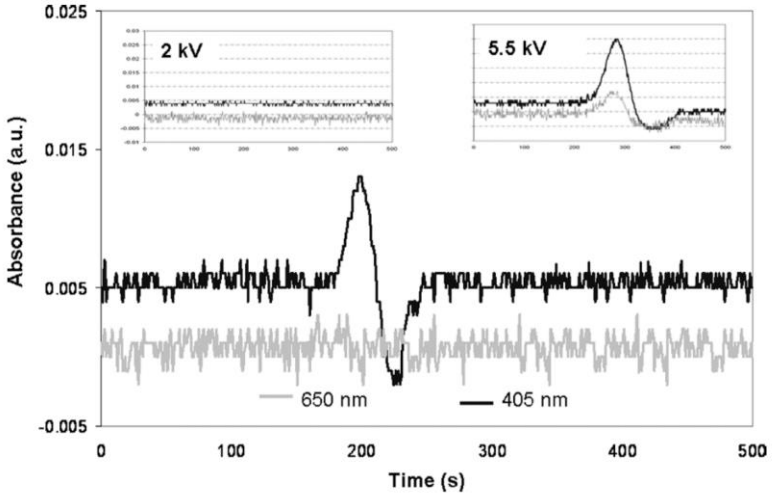

Figure 2.8. Myoglobin exclusion negative peak. Demonstration of a protein exclusion with anode at entrance [41], resulting in polarity opposite that described in Section 2.3.2 of the present study.

2.4 Concluding remarks

This work described the development of a separation technique termed electrophoretic exclusion, capable of simultaneous capture and enrichment of species near a reservoir-channel interface. A capillary-based device with interfacial electrode was designed and fabricated for use in the proof-of-concept studies using the electrophoretically mobile dye methyl violet. Successful capture and concentration of methyl violet within the proximity of the entrance was demonstrated. Indirect analysis of the electric field effects inside the channel versus at the entrance suggested a more prominent electric field influence near the entrance that warrants further investigation. A discussion relating to the observed negative peaks and their possible causes was also provided. Electrophoretic exclusion offers the unique possibility of simultaneous separation and concentration in bulk solution but relies heavily on the velocity and electric fields at the channel entrance.

2.5 References

[1] Lottspeich, F. *Electrophoresis* 2008, *29*, 2449-2450.

[2] Shintani, H., Polonsky, J., Editors. 1997, 737.

[3] Linhardt, R. J., Toida, T. *Science* 2002, *298*, 1441-1442.

[4] Klodzinska, E., Buszewski, B. *Anal. Chem. (Washington, DC, U. S.)* 2009, *81*, 8-15.

[5] Jorgenson, J., Lukacs, K. *Anal. Chem.* 1981, *53*, 1298-1302.

[6] Jorgenson, J., Lukacs, K. *J. Chromatogr.* 1981, *218*, 209-216.

[7] Jorgenson, J., Lukacs, K. *Science* 1983, *222*, 266-272.

[8] Karger, B., Cohen, A., Guttman, A. *J. Chromatogr. -Biomed. Appl.* 1989, *492*, 585-614.

[9] Issaq, H. *Electrophoresis* 1999, *20*, 3190-3202.

[10] Sia, S., Whitesides, G. *Electrophoresis* 2003, *24*, 3563-3576.

[11] Kuehnbaum, N. L., Britz-McKibbin, P. *Chem. Rev.* 2013, *113*, 2437-2468.

[12] Albin, M., Grossman, P. D., Moring, S. E. *Anal. Chem.* 1993, *65*, 489A-497A.

[13] Breadmore, M. C. *Journal of Chromatography a* 2012, *1221*, 42-55.

[14] Breadmore, M., Haddad, P. *Electrophoresis* 2001, *22*, 2464-2489.

[15] Breadmore, M. C. *Electrophoresis* 2007, *28*, 254-281.

[16] Breadmore, M. C., Thabano, J. R. E., Dawod, M., Kazarian, A. A. *et al*. *Electrophoresis* 2009, *30*, 230-248.

[17] Mala, Z., Gebauer, P., Bocek, P. *Electrophoresis* 2011, *32*, 116-126.

[18] Breadmore, M. C., Dawod, M., Quirino, J. P. *Electrophoresis* 2011, *32*, 127-148.

[19] Chen, Y., Lu, W., Chen, X., Teng, M. *Central European Journal of Chemistry* 2012, *10*, 611-638.

[20] Breadmore, M. C., Shallan, A. I., Rabanes, H. R., Gstoettenmayr, D. *et al*. *Electrophoresis* 2013, *34*, 29-54.

[21] Breadmore, M. C., Tubaon, R. M., Shallan, A. I., Phung, S. C. *et al*. *Electrophoresis* 2015, *36*, 36-61.

[22] Mikkers, F. E. P., Everaerts, F. M., Verheggen, T. P. E. M. *Journal of Chromatography A* 1979, *169*, 1-10.

[23] Gebauer, P., Thormann, W., Bocek, P. *J. Chromatogr.* 1992, *608*, 47-57.

[24] Gebauer, P., Thormann, W., Bocek, P. *Electrophoresis* 1995, *16*, 2039-2050.

[25] Aebersold, R., Morrison, H. *J. Chromatogr.* 1990, *516*, 79-88.

[26] Britz-McKibbin, P., Bebault, G., Chen, D. *Anal. Chem.* 2000, *72*, 1729-1735.

[27] Shackman, J. G., Ross, D. *Electrophoresis* 2007, *28*, 556-571.

[28] Giddings, J. C., Dahlgren, K. *Separation Science* 1971, *6*, 345-356.

[29] Ofarrell, P. H. *Science* 1985, *227*, 1586-1589.

[30] Greenlee, R. D., Ivory, C. F. *Biotechnol. Prog.* 1998, *14*, 300-309.

[31] Koegler, W. S., Ivory, C. F. *Biotechnol. Prog.* 1996, *12*, 822-836.

[32] Koegler, W. S., Ivory, C. F. *Journal of Chromatography a* 1996, *726*, 229-236.

[33] Huang, Z., Ivory, C. F. *Anal. Chem.* 1999, *71*, 1628-1632.

[34] Ross, D. *Anal. Chem. (Wash.)* 2002, *74*, 2556-2564.

[35] Shackman, J. G., Munson, M. S., Kan, C., Ross, D. *Electrophoresis* 2006, *27*, 3420-3427.

[36] Hori, A., Matsumoto, T., Nimura, Y., Ikedo, M. *et al*. *Anal. Chem.* 1993, *65*, 2882-2886.

[37] Polson, N. A., Savin, D. P., Hayes, M. A. *J. Microcolumn Sep.* 2000, *12*, 98-106.

[38] Pacheco, J. R., Chen, K. P., Hayes, M. A. *Electrophoresis* 2007, *28*, 1027-1035.

[39] Meighan, M. M., Keebaugh, M. W., Quihuis, A. M., Kenyon, S. M., Hayes, M. A. *Electrophoresis* 2009, *30*, 3786-3792.

[40] Han, J., Chun, M., Riaz, A., Chung, D. *Electrophoresis* 2005, *26*, 480-486.

[41] Meighan, M. M., Vasquez, J., Dziubcynski, L., Hews, S., Hayes, M. A. *Anal. Chem.* 2011, *83*, 368-373.

[42] Beckers, J., Everaerts, F. *J. Chromatogr. A* 1997, *787*, 235-242.

[43] Gebauer, P., Bocek, P. *J. Chromatogr. A* 1997, *772*, 73-79.

[44] Desiderio, C., Fanali, S., Gebauer, P., Bocek, P. *J. Chromatogr. A* 1997, *772*, 81-89.

[45] Gebauer, P., Pantuckova, P., Bocek, P. *Anal. Chem.* 1999, *71*, 3374-3381.

[46] Gas, B., Hruska, V., Dittmann, M., Bek, F., Witt, K. *Journal of separation science* 2007, *30*, 1435-1445.

[47] Squires, T., Bazant, M. *J. Fluid Mech.* 2004, *509*, 217-252.

[48] Yossifon, G., Frankel, I., Miloh, T. *Phys. Fluids* 2006, *18*, 117108.

[49] Takhistov, P., Duginova, K., Chang, H. C. *J. Colloid Interface Sci.* 2003, *263*, 133-143.

Chapter 3

Quantitative assessment of flow and electric fields

3.1 Introduction

Since its inception capillary electrophoresis (CE) has matured into a highly efficient analytical technique amenable to multiplexed, microfluidic separations of compounds and biomolecules from complex samples [1-3]. Despite its advantages, the low concentration sensitivity with typical CE and related techniques remains a major drawback [4]. This has spurred an interest in methods designed to improve sensitivity without compromising the distinguishing benefits of electrophoretic separations. Many techniques have relied on the equilibrium gradient principle summarized by Giddings [5] to achieve the improved sensitivity. Here, constant forces opposed to a gradient cause a unique and specific equilibrium position to where analytes with similar properties, such as net charge, mass, size, etc., migrate to from all parts of the separation domain. Separation and concentration occur simultaneously and diffusional band-broadening is minimized as restoring forces on both sides of the equilibrium position act to keep the concentration plug focused. Isoelectric focusing (IEF) [6, 7], counteracting chromatographic electrophoresis (CACE) [8], electric field gradient focusing (EFGF) [9], and temperature gradient focusing (TGF) [10], to name a few, have all successfully exploited the equilibrium gradient technique by establishing continuous in-channel gradients to separate analytes serially within the confines of a channel.

Other techniques have been developed to establish a focusing condition near a converging channel entrance where fluid velocity and electric field gradients typically exist. Many of these designs were primarily developed for the purpose of pre-

concentrating all analytes for injection into a channel for further electrophoretic separation, and consequently little attention was given to the possibility of separation selectivity at the entrance region [11-13]. Some works, however, explored the feasibility of exploiting the relatively sharp field gradient at the entrance to create a selective focusing condition. Under these conditions, some analytes of a particular electrophoretic (EP) mobility could be excluded from entering the channel and concentrated in an inlet buffer reservoir, while other analytes, with different EP mobilities, pass through to an exit reservoir [14-17]. The separation condition described here is fundamentally different from the techniques that create a continuous gradient to separate analytes serially along the gradient. Rather, this technique is designed to establish a single differentiation zone that would be of little value as a stand-alone separation tool, but could be of significant value in a serial or parallel (array) format where the electric field and detection element of each array unit could be specifically tailored and independently operated to concentrate a chosen category of analytes in bulk solution.

Works to establish the exclusion condition at the entrance have predominantly used traditional CE electrode configurations, where the anode and cathode electrodes are placed in the buffer reservoir away from the channel entrance and exit [14-17]. It is presumed that with this configuration, flow and electric field gradients largely overlap, thereby increasing the complexity of optimizing a discrete, high resolution separation zone at the entrance. Pacheco *et al*. [18] numerically described the 2D model of an earlier exploratory electrophoretic focusing experiment [19], where an electrode was placed exactly at the reservoir-channel entrance interface with the intent of decoupling the electric field gradient from the flow field gradient by confining the electric field more to

the channel (Figure 1). Work using a similar configuration demonstrated qualitative differential behavior at the interface leading to separation and concentration enhancement of small molecules [20] and proteins [21]. However, unlike IEF, CACE, EFGF, and TGF that have been extensively modeled and tested empirically to help improve performance and increase the overall understanding of gradient field separations within a channel [22, 23], little detailed quantitative experimental information exists for the combined effects of the flow and electric field gradients at a channel entrance, particularly where an electrode is in close proximity to the entrance. There is a strong need to confirm or contradict intuitive and theoretical understanding of this entrance area so that any future progress can be built upon a solid foundation.

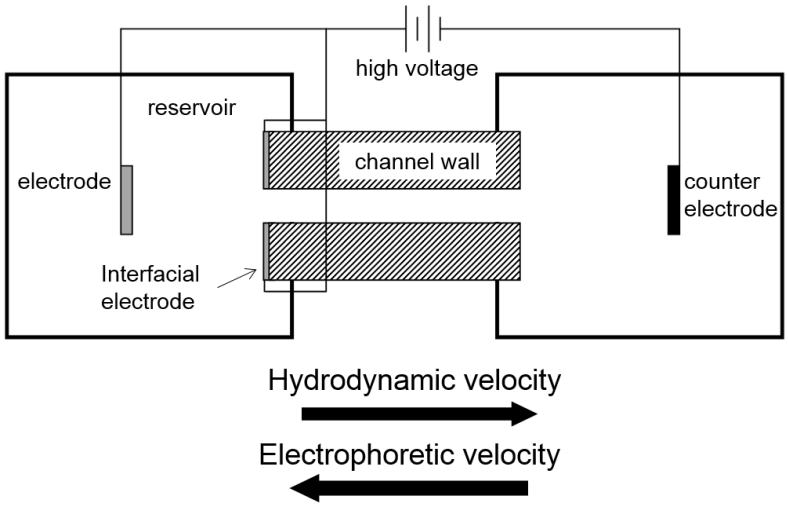

Figure 3.1. Schematic of electrophoretic focusing principle with the interfacial electrode configuration described in this work.

This work uses the velocities of charged particles to investigate the hydrodynamic and electrokinetic effects in the region adjacent to the channel entrance (Figure 3.1). Both particle image velocimetry (PIV) and particle tracking velocimetry (PTV) studies with charged fluorescent particles have been used to monitor fluid and EP-influenced

velocities [24, 25]. A 3D model specific to the fabricated device was developed using finite element analysis software and utilized to simulate the principle of electrophoretic focusing at the channel entrance. In order to assess the particle tracking methodology and the accuracy of a model in predicting hydrodynamic gradients, PTV was first used to measure particle velocities in the device when only hydrodynamic flow was present. Subsequently, varying electric fields were applied to create an electrokinetic force counter to the hydrodynamic force in an effort to evaluate the combined gradient effects. Results showed a non-linear hydrodynamic flow gradient near the channel entrance was accurately described using the model for this specific system. In the same region of interest, stepped increases in the electric field caused decreases in net particle velocities consistent with model simulations.

3.2 Materials and methods

3.2.1 Device fabrication

A 144 μL glass plate reservoir was fabricated by placing a 360 μm spacer between two 2 cm glass squares cut from standard microscope slides and epoxying the perimeter (Figure 3.2A). Four syringe needles with removable caps (Exel International, St. Petersburg, FL, USA) were inserted at each corner to serve as inlets or outlets and to facilitate cleaning when necessary. The cleaved tips of four fused silica capillaries (5 cm in length, 75 μm i.d. 365 μm o.d., Polymicro Technologies, Phoenix, AZ, USA) had a small portion (~0.5 cm) of the polyamide coating removed and were sputter-coated with 30 nm titanium then 50 nm platinum. The sputtered capillary face served as an electrode symmetric to and exactly at the capillary channel entrance. The electrode faces were electrically connected to a platinum wire by aligning the tips parallel to one another and

fixing their sputtered sides with silver conducting epoxy. All conducting surfaces with the exception of the electrode faces were coated with standard epoxy to render them electrically nonconductive and nonreactive in solution. The electrode ends of the capillary bundle were inserted and fixed into the fabricated glass plate reservoir and the non-sputtered ends were inserted and fixed into a 2 mL glass outlet vial. A platinum electrode was set 1 cm external to the capillary face electrode in the plate reservoir and a counter electrode was placed in the 2 mL outlet vial.

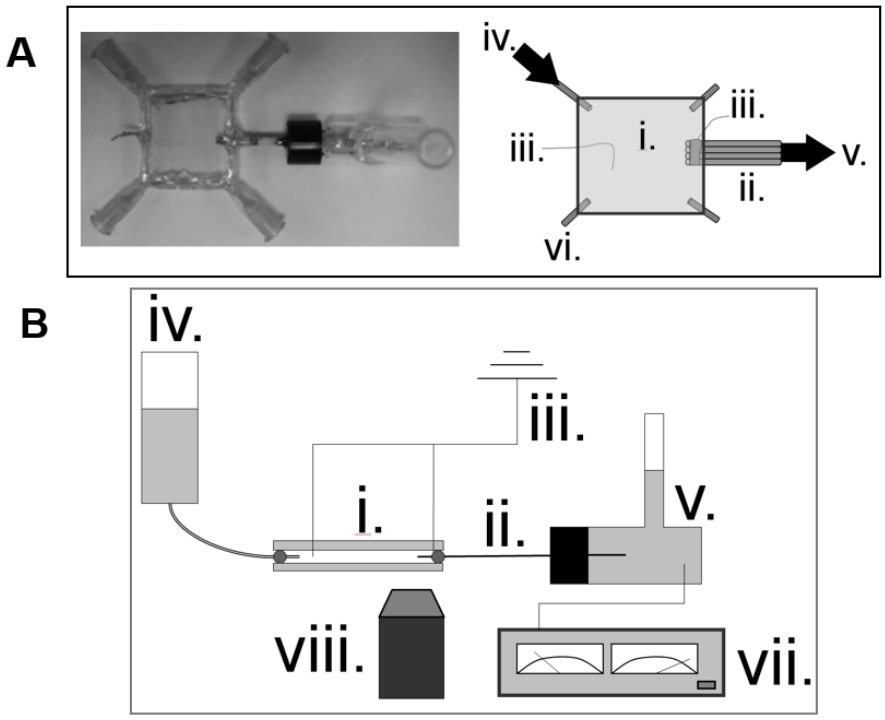

Figure 3.2. (A) Top-view photo and schematic of glass plate device fabricated to image particles near a converging channel with electrode exactly at entrance. Hydrodynamic flow was from left inlet to right outlet. (B) Side-view schematic of experimental setup. A CCD camera attached to an epifluorescence microscope was used to capture fluorescent particle images. (i.) glass plate reservoir (ii.) 4-capillary bundle (iii.) electrode (iv.) inlet (v.) outlet (vi.) additional inlets/outlets (vii.) power supply (viii.) objective

3.2.2 Particle tracking experiments

Velocimetry data from four identical capillaries connected in parallel were compiled and treated as one dataset for the study. Buffer was prepared to 5 mM using DL aspartic acid (Sigma Aldrich, St. Louis, MO, USA) and18 MΩ water then adjusted to pH 2.80 using 1 M HCl (Mallinckrodt, Hazelwood, MO, USA). Ten microliters of stock sulfated fluorescent polystyrene particles of 1 μm diameter and 505/515 wavelength excitation/emission (Invitrogen, Carlsbad, CA, USA) were diluted to 2 mL with working buffer and sonicated for 15 minutes, yielding a concentration of approximately 2×10^8 particles/mL. Particles had an EP mobility of 3.5×10^{-4} $cm^2/(Vs)$ as determined from previous experiments using similar conditions [26] . The inlet vial, glass plate reservoir, capillary bundle, and outlet vial were preconditioned with 0.1 M HCl for 10 minutes then flushed with the working buffer for 20 minutes by pressurizing the inlet with house nitrogen. Preconditioning [27] and low pH buffer [28] helped limit EOF to simplify flow conditions and quantification of the system. The 2×10^8 particles/mL suspension was introduced into the reservoir by adding 100 μL to 4 mL of working buffer in the inlet vial and pressurizing with nitrogen. The pressurized inflow aided the mixing and uniform particle distribution throughout the reservoir. The final particle concentration in the reservoir was approximately 5×10^6 particles/mL. Pressure was removed, and bulk flow for the experiments was established and controlled using hydrostatic pressure created by keeping the inlet fluid level higher than that of the outlet, forcing particles to flow through the channels (Figure 3.2B). The average system flow rate of 2.7 nL/s was calculated using the hydrostatic pressure change from the 19 mm fluid level difference [1.9×10^5 $g/(ms^2)$] and total hydrodynamic resistance of the inlet, reservoirs, and

channels [6.9 x 10^{16} g/(m^4s)]. It was assumed the flow rate in each of the four capillaries was one-fourth the total flow rate, or 0.68 nL/s, due to flow division common in parallel, like-channel configurations. The duration of the study totaled 19 min, equating to a 1% hydrodynamic flow rate change as a result of inlet and outlet fluid levels changing over time. For the electrokinetic studies, the cathode in the outlet vial was attached to a Bertan Series 225 power supply (Bertan, Hauppauge, NY, USA), and both anodes in the glass plate reservoir were held to ground. Electric potential was applied incrementally from 0-200 V across the channel to create global electric fields ranging from 0-40 V/cm.

Particles were imaged using an Olympus IX70 inverted epifluorescence microscope (Tokyo, Japan) with a 4x, UPlanAPO, 0.16 NA objective and mercury short arc light source. Image acquisition was achieved using a QICAM CCD camera (QImaging, Burnaby, Canada) and Streampix III image capturing software (Norpix, Montreal, Quebec, Canada) set to 45 ms exposure time with an average frame rate of 16 frames per second and 1.8 mm x 1.6 mm imaging region (the minimum required to image all 4 capillaries at once) focused on the longitudinal mid-plane of the 4 capillary entrances. The exposure time of 45 ms remained constant throughout the experiment and was selected during test trials to maximize fluorescence intensity of the particles while simultaneously limiting particle streaks (particle images longer than 5 um) to only a few microns from the channel interface where particle velocities increase rapidly. Images were recorded for a total of 60 s during each measurement, with voltage applied after the initial 10 s in the case of the electrokinetic studies.

3.2.3 Image analysis

The MTrackJ plugin within ImageJ software (http://rsbweb.nih.gov/ij/) was used to manually track and determine the velocity of the particles. Each particle was cursor-selected throughout each advancing frame assigning it a coordinate that was used to determine distance traveled over the frame interval. For all images, a 100 μm long x 25 μm high region in the reservoir directly adjacent to the center of the channel entrance was selected and only particles moving within this zone were tracked to reduce velocity variations from particles outside the ± 12.5 um centerline region. The microscope objective was focused at the z-plane bisecting the channel, so particles outside the 25 um depth of focus would have a fluorescent diameter greater than 5 μm and would be excluded. A total of 204 particles were tracked over the course of the data collection, with at least 40 in-focus and traceable particles passing through the region of interest during the 0, 50, 100, and150 V trials and 18 for the 200 V trial.

3.2.4 Model development

The fabricated device used in this study was modeled using COMSOL Multiphysics 4.2 software with the microfluidics module (COMSOL, Inc., Los Angeles, CA, USA). The device materials - liquid, silica glass, and platinum – were selected from the built-in library and assigned to the respective geometric entities. The liquid electrical conductivity was modified to reflect that of the aspartic acid buffer (0.04 S/m) used in the experiments. Ohm's Law and the Navier-Stokes equation were solved for by assigning Electric Current and Laminar Flow interfaces to the respective domains. Electric potential was assigned to an electrode boundary located 1 mm from the exit in the reservoir, while ground was assigned to the electrode boundary on the capillary face and

to an electrode boundary located 1 mm from the entrance in the reservoir. All other boundaries were defined as electrical insulation. Laminar, incompressible flow was assigned to all domains and a no slip condition used for all wall boundaries. The laminar inflow boundary condition was set to a flow rate of 0.68 nL/s to match that of the PTV experiments. A 3.5×10^{-4} $cm^2/(Vs)$ EP mobility (from section 2.2) and global 700 V applied potential (for 3.1) were used to calculate EP velocities.

With the high aspect ratio geometry of the device, the reservoir length (2 cm) and width (2 cm) dimensions were scaled down by a factor of 20, having no noticeable effect on the gradient fields near the channel entrance. Channel length (5 cm) was reduced by a factor of 100, having a linear scaling effect on electric field near the entrance that was easily rescaled after computation. The scaling effects were determined by comparing the simulation results from the original dimensions to the simulation results from several scaled geometries. Scaled dimensions were used to improve mesh quality and computation performance. All other model parameters closely mirrored the fabricated device and experimental conditions.

Before developing the 3D model that more accurately reflected the geometry of the fabricated device, a 2D model (not shown) was developed using the COMSOL program to validate against the similar 2D theoretical development described by Pacheco *et al*. [18]. As expected, the resulting numerical descriptions of the fields that define the gradient near the channel entrance were reasonably consistent between the different modeling approaches, motivating the expansion of the 2D model to 3D using the COMSOL program.

3.3 Results and discussion

3.3.1 Model development and simulated principle of electrophoretic focusing

The 3D model was used to generate centerline velocities for comparison with particle tracking data. The resulting 300 μm/s fully-developed flow velocity from the simulation (Figure 3.3B) was consistent with the centerline velocity calculated using the Poiseuille equation. Beyond the hydrodynamic flow, other critical parameters used in the simulations, and required for electrophoretic focusing within the inlet reservoir, include the globally applied electric field and the EP mobility of the species of interest. When the average EP velocity towards the reservoir becomes equal to the average hydrodynamic velocity towards the channel at any location where $x \leq 0$ (denoted in Pacheco *et al*. as S = 1 locally [18]), the cross-sectionally averaged mass flux of an analyte is zero (including diffusive elements) and a focusing condition occurs. Because average EP mobility of the species remains constant for the given buffer, the focusing behavior could be controlled by varying the hydrodynamic flow and/or electric field. The net velocity plot, which is the sum of two opposing centerline velocities, reached a focusing condition ($y = 0$) a few microns outside the channel entrance and inside the inlet reservoir (Figure 3.3A).

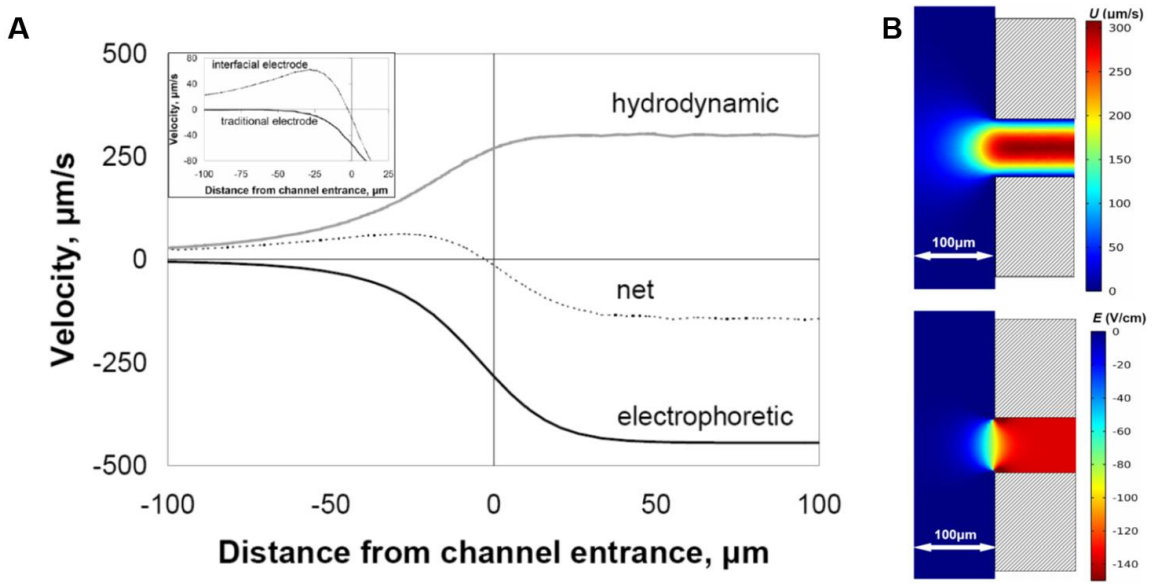

Figure 3.3. (A) Simulation showing the principle of electrophoretic exclusion at a channel entrance with an electrode exactly at the reservoir-channel interface. The central dashed line represents the net velocity resulting from electrophoretic velocity opposing bulk fluid velocity. (Inset) The net velocity with an interfacial electrode configuration, as described in A, compared to the net velocity profile of a traditional CE configuration, where no interfacial electrode is present. All plots reflect centerline values. (B) Surface plot simulations of fluid velocity, *U*, from 0.68 nL/s applied flow rate and electric field, *E*, from 700 V applied potential at a converging channel entrance with interfacial electrode.

The placement of the electrode in the reservoir was examined theoretically. A magnified region of the net velocity profile was examined (Figure 3.3A – inset) with the electrode placed distal (traditional CE configuration) and at the entrance (Figure 3.1). Two major effects on the velocity profile were noted when the electrode resided exactly at the entrance. First, the electric field had minimal influence on the net velocity until roughly 25 μm from the entrance. Having an electrode at the entrance and another held at the same potential in the reservoir ensured an almost zero electric field across the reservoir except near the entrance where focusing is designed to occur. Secondly, unlike the traditional CE electrode configuration (Figure 3.3A – inset, lower black line), there

was a much steeper velocity gradient induced by the electric field being confined near the channel entrance, indicating a steeper local gradient in *E* in the presence of a flow field. This describes a microscale gradient electrophoresis system where bandwidth is inversely proportional to the gradient. The steeper gradient suggests that any resulting concentration profile generated by the focusing condition will be narrower. This is analogous to pH gradients in isoelectric focusing but with steeper gradients and without dynamic range limitations since each interface is designed to differentiate a single species of interest.

3.3.2 Assessment of hydrodynamic velocity gradient using PTV and simulation

Particle tracking velocimetry was used near the channel entrance in order to evaluate the flow field as compared to the model. As the particles approached the channel entrance along the centerline, the distance between the tracking points over a constant frame interval became larger, indicating a fluid velocity gradient (Figure 3.4A). In most cases, it was possible to track the particles to within 5 μm of the reservoir-channel interface before they disappeared inside the capillary within the next frame. The velocity trend of the particles in the gradient region agreed with that predicted by the model simulation when no electric field was present (Figure 3.4B).

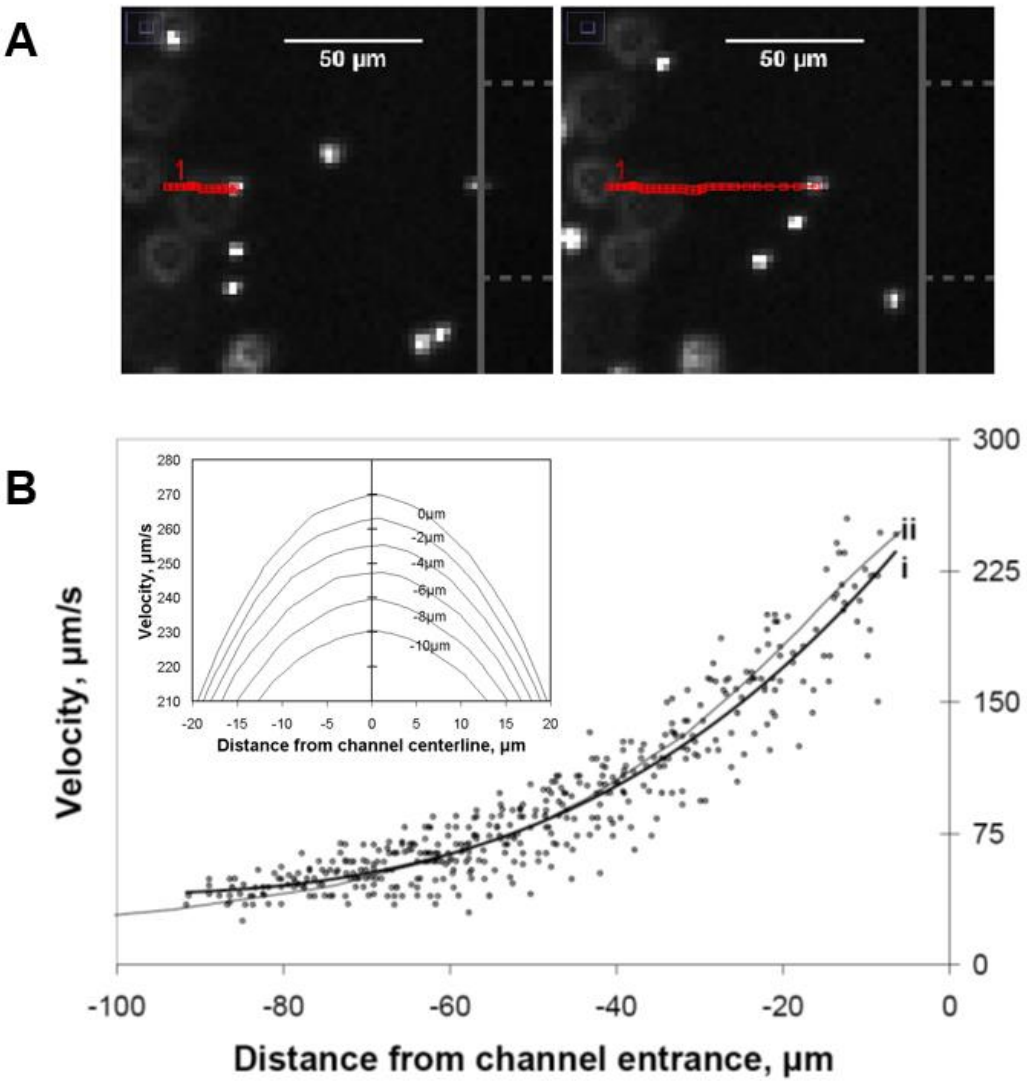

Figure 3.4. (A) Representative snapshot of manually tracked fluorescent particle moving left to right and approaching channel entrance along centerline. Open (red) squares represent particle location in prior frames. Capillary face and channel are represented by solid vertical line and dashed horizontal lines, respectively, along right edge of panel. The elapsed time between the two snapshots was 0.88 s. (B) Centerline velocity plot of fluorescent particles as they approached the capillary entrance (x = 0) as in A. Line (i) is the best fit for the data points, and line (ii) is the centerline fluid velocity plot from the 3D model. (B - inset). Simulated velocity profiles about the centerline from 0 to -10 um that illustrate velocity variation off the centerline near the channel entrance (applied U = 0.68 nL/s).

Scatter amongst the velocities was mostly attributed to particles several microns off the *y*- and *z*- center planes being included in the centerline tracking data. The error associated with the distances off the centerline and near the entrance was predicted using the simulation (Figure 3.4B – inset). Taking into account the width of the region of interest and the depth of focus of the microscope objective (section 2.3), a ±18% relative standard deviation could be expected in measurements occurring -7.5 μm from the interface.

3.3.3 Assessment of combined electric field and hydrodynamic velocity gradients using PTV and simulation

Charged species in the presence of flow and electric gradients near the channel entrance were examined next. With the flow velocity field quantified from the previous section, any change in particle velocity is assumed to be a direct result of the electric field. Hydrostatic conditions were held constant throughout and particle velocity control images were captured before each applied potential. A consistent decrease in net velocity as a result of the increasing electric field was evident (Figure 3.5A).

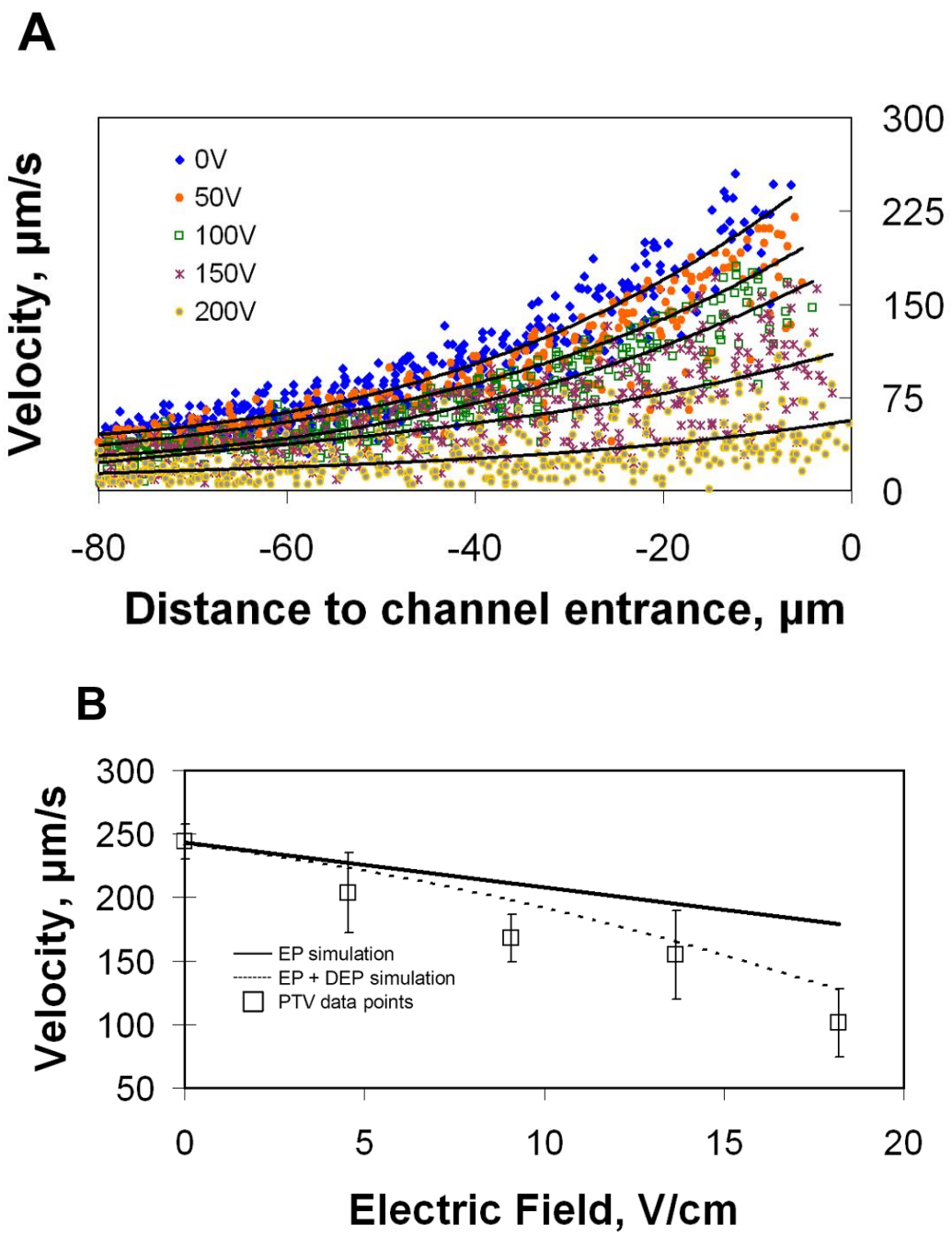

Figure 3.5. (A) Particle velocities approaching channel entrance (x = 0) along centerline with increasing applied electric potentials. (B) Average velocity of particles in electric fields at -7.5 ± 1.5 µm from channel entrance. Each data point is the mean of 3 to 19 tracked particles with 1 sigma error bars. The solid line represents a simulation where only electrophoretic velocity was considered while the dashed line includes both electrophoretic (EP) and dielectrophoretic (DEP) forces.

To illustrate the relationship between velocity and electric field in this system, a bin -7.5 ± 1.5 μm outside the entrance (where particles were still visible and velocity could be tracked) was chosen (Figure 3.5B). Using the model and combining the electric field and flow effects at -7.5 μm, an estimated net velocity was calculated for the various applied electric field strengths. The velocities from the experimental data decreased with increased electric field but at a greater slope than the simulation. EOF was not likely the cause of this behavior because preconditioning and low pH buffer (as described in the methods section) severely limited these effects. Additionally, based on the experimental conditions, EOF would have countered the EP velocity making the slope shallower rather than steeper. Dielectrophoresis, on the other hand, was considered a viable explanation for the discrepancy since this force typically has a more pronounced effect at higher electric field gradients, and since the particles used were known to be polarizable and of an appropriate size to generate a non-trivial force. The dielectric force is proportional to the local electric field gradient squared and particle radius to the third power and is described in detail elsewhere [29, 30] . To examine this possibility quantitatively, the force was calculated within the construct of the 3D model using a dielectrophoretic mobility of -2×10^{-8} $cm^4/(V^2s)$ [26] (Figure 3.5B). The addition of the dielectrophoretic effects provided an improved fit to the data and was likely a factor. The core flow and electric field effects can still be interpreted from this data, however, as the dielectrophoretic effects are well-studied, quantifiable, and can be considered an artifact as a result of the physical properties of the particles which are required as tracers. Small molecules, peptides and proteins - the putative targets for this system - will have negligible dielectrophoretic susceptibilities.

Though the motivation for the current work was to quantify the gradient region near an entrance rather than demonstrate a full exclusion condition, an earlier proof-of-principle study was carried out with stronger electric fields to verify that a charged substance could be slowed and eventually excluded from entering the channel (Figure 3.6).

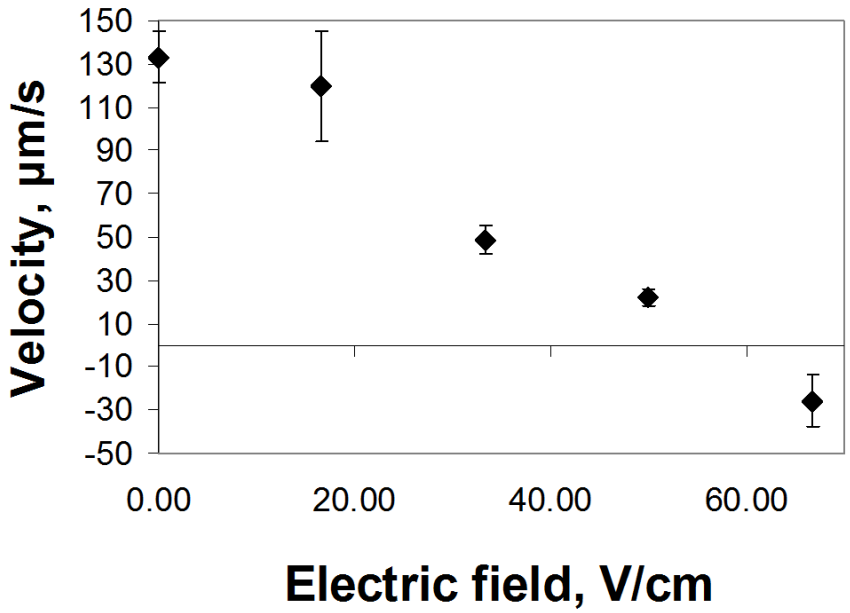

Figure 3.6. Particle velocities approaching channel entrance (x=0) along centerline with increasing applied electric potentials similar to Figure 5 but showing full reversal of the particle direction. The reservoir in this setup was a 2 mL glass vial rather than the two parallel glass plates, creating interfering background fluorescence that limited the number of particles that could be tracked. The electric field shown on the x-axis is simply the applied potential divided by 12 cm, the length of the capillary for this study. However, modeling results indicate that the field near the entrance where the particles are tracked would be about half the fully developed field inside the capillary channel.

3.4 Concluding remarks

To begin to investigate and rationally alter an electrified converging flow interface, quantitative models and data must be generated and compared. Using a highly symmetric and traditional interface with an electrode positioned at the entrance, a model was generated and data collected with particle tracers to investigate both the interface and

the accuracy of the model. For this interface, the model and data agree and the strategy is validated. This work enables logical and informed device design, like shaping the entrance geometry or placing the electrode at different locations, and similar strategies for models and velocity visualization can be used to optimize separation conditions at a channel entrance.

3.5 References

[1] Jorgenson, J. W., Lukacs, K. D. *Science* 1983, *222*, pp. 266-272.

[2] Linhardt, R. J., Toida, T. *Science* 2002, *298*, 1441-1442.

[3] Lottspeich, F. *Electrophoresis* 2008, *29*, 2449-2450.

[4] Albin, M., Grossman, P. D., Moring, S. E. *Anal. Chem.* 1993, *65*, 489A-497A.

[5] Giddings, J. C., Dahlgren, K. *Separation Science* 1971, *6*, 345-356.

[6] Righetti, P. G., Drysdale, J. W. *Isoelectric focusing*, Amsterdam, North-Holland Pub. Co. 1976.

[7] Kolin, A. *Proc. Natl. Acad. Sci. U. S. A.* 1955, *41*, 101-10.

[8] O'Farrell, P. H. *Science* 1985, *227*, pp. 1586-1589.

[9] Koegler, W. S., Ivory, C. F. *Journal of Chromatography A* 1996, *726*, 229-236.

[10] Ross, D. *Anal. Chem. (Wash.)* 2002, *74*, 2556-2564.

[11] Astorga-Wells, J. *Anal. Chem. (Wash.)* 2003, *75*, 5207-5212.

[12] Wu, X. *Anal. Chem. (Wash.)* 1998, *70*, 2081-2084.

[13] Wei, W. *Anal. Chem. (Wash.)* 2002, *74*, 3899.

[14] Hori, A., Matsumoto, T., Nimura, Y., Ikedo, M. *et al*. *Anal. Chem.* 1993, *65*, 2882-2886.

[15] McLaren, D. *Anal. Chem. (Wash.)* 2004, *76*, 2298.

[16] Wang, Q., Yue, B., Lee, M. L. *Journal of Chromatography A* 2004, *1025*, 139-146.

[17] Shackman, J. *Anal. Chem. (Wash.)* 2007, *79*, 565-571.

[18] Pacheco, J. R., Chen, K. P., Hayes, M. A. *Electrophoresis* 2007, *28*, 1027-1035.

[19] Polson, N. A., Savin, D. P., Hayes, M. A. *J. Microcolumn Sep.* 2000, *12*, 98-106.

[20] Meighan, M. M., Keebaugh, M. W., Quihuis, A. M., Kenyon, S. M., Hayes, M. A. *Electrophoresis* 2009, *30*, 3786-3792.

[21] Meighan, M. M., Vasquez, J., Dziubcynski, L., Hews, S., Hayes, M. A. *Anal. Chem.* 2011, *83*, 368-373.

[22] Meighan, M. M., Staton, S. J., Hayes, M. A. *Electrophoresis* 2009, *30*, 852-865.

[23] Kenyon, S. M., Meighan, M. M., Hayes, M. A. *Electrophoresis* 2011, *32*, 482-493.

[24] Devasenathipathy, S. *Anal. Chem. (Wash.)* 2002, *74*, 3704-3713.

[25] Devasenathipathy, S., Santiago, J. G., Wereley, S. T., Meinhart, C. D., Takehara, K. *Exp. Fluids* 2003, *34*, 504-514.

[26] Weiss, N. *Electrophoresis* 2011, *32*, 2292-2297.

[27] Han, J. *Electrophoresis* 2005, *26*, 480-486.

[28] He, Y., Lee, H. K. *Anal. Chem.* 1999, *71*, 995-1001.

[29] Pohl, H. *J. Appl. Phys.* 1951, *22*, 869-871.

[30] Chen, K. P., Pacheco, J. R., Hayes, M. A., Staton, S. J. *Electrophoresis* 2009, *30*, 1441-1448.

Chapter 4

Localized asymmetric electric and velocity field effects during counter-flow gradient focusing at a converging channel

4.1 Introduction

The appeal of CE and related microfluidic electrophoresis separations often stems from the high resolution, low volume reagent use, and highly adaptable simple designs common with most systems. However, limited sensitivity has been historically regarded as a major drawback to the technique [1]. Consequently, a variety of on-line concentration enhancement strategies have been developed to overcome this issue [2-7].

Sample stacking, broadly defined as analyte concentration enhancement on a boundary by electrophoretic (EP) velocity change, is one such strategy which encompasses a variety of configurations [4, 8-10]. Among the simplest and most common configuration is on-line field-amplified sample stacking (FASS). FASS results when two solutions of different conductivity induce an electric field gradient at the solution boundary to where electrophoretically mobile analytes migrate, stack, and are subsequently separated using traditional CZE [11]. While this configuration has been widely accepted for on-line pre-concentration of charged analytes within the sample, it is largely dependent on the sample amount initially injected and limited by the conductivity ratio between the two solutions [10].

Counter-flow gradient focusing offers another general sample stacking approach that relies on the equilibrium gradient principle, summarized by Giddings, to achieve the improved sensitivity [12]. While the specifics of several focusing configurations have been described elsewhere [13, 14], all employ a constant force opposed to some gradient

(electric field, pH, conductivity, temperature, micelle, etc.) to cause a unique and specific equilibrium position to where analytes with similar properties, such as net charge, mass, size, etc., migrate from all parts of the separation domain. Separation and concentration occur simultaneously and diffusional band-broadening is minimized as restoring forces on both sides of the equilibrium position act to keep the concentration plug focused.

Electrophoretic exclusion is a form of counter-flow gradient focusing where charged analytes with constant hydrodynamic velocities (U) oppose an electrophoretic velocity (U_{EP}) induced by an electric field residing at a channel entrance [15-17]. Generally speaking, when an exclusion condition exists for a given analyte, the analyte velocity drops to zero at the equilibrium boundary where it concentrates and never enters the channel. Analytes with higher EP mobility are also excluded from entering the channel while analytes with lower EP mobility pass through the entrance boundary until they exit the opposite channel end. Unlike FASS or related stacking techniques that rely on a conductivity ratio between solution plugs to create an electric field gradient, and unlike most other counter-flow gradient focusing techniques that create a continuous gradient to separate analytes serially along the gradient, electrophoretic exclusion relies on distinct electric field and flow field gradients induced at a converging channels entrance with deliberately positioned electrodes to create a single differentiation zone. Advantages offered by this design include simultaneous separation and concentration that is not limited to creating and maintaining conductivity ratios near the entrance. Additionally, this design can be easily expanded to serial or parallel (array) formats where the electric field and detection element of each array unit could be specifically tailored and independently operated to concentrate a chosen category of analytes in bulk

solution. However, the effectiveness of this design is heavily dependent on the shape and steepness of the field gradients [18].

The significance of the entrance geometry and spatial arrangement of the electric field and hydrodynamic velocity gradients for electrophoretic exclusion and related techniques has been realized [16, 19]. The coupling of simulated electrophoretic and fluid velocity fields along a longitudinal entrance centerline demonstrated an electric field gradient sharpening effect with an electrode placed about the entrance, although the entrance geometry as a whole was ignored [20]. An electrode with no radial symmetry and patterned a few micrometers from the entrance of a PDMS microdevice produced a gradient still capable of achieving electrophoretic exclusion, but the specific impact of symmetry and location on performance was not quantified [21]. In a recently published theoretical description of the electrophoretic exclusion construct, resolution was found to be directly dependent on the steepness of the electric field gradient at the entrance [18]. Despite the useful information obtained from the previous studies, evidence exists that flow and electric field gradients also vary laterally across the entrance, especially near the walls and corners, necessitating further examination of this region to better understand the field gradient components that directly affect the exclusion condition [16, 20].

This work examines the lateral fluid velocity and electric fields within the channel entrance region by simulation and experiment to aid future device design and fabrication strategies. A model using finite element analysis was constructed to perform simulations with experimentally-similar electrophoretic exclusion conditions in an effort to extrapolate information pertaining to lateral electric fields, fluid velocity fields, and any transport dynamics that may be associated with diffusion, convection, and electrokinetic

dispersion. To experimentally assess the gradient field and transport effects for comparison to the simulation, the concentration of charged fluorescent dye was monitored at the entrance using fluorescent microscopy and midway down the channel with visible spectroscopy. Simulation and experimental results were consistent and indicated decreased gradient uniformity for both electric and fluid velocity fields closer to the channel wall that resulted in a localized concentration enhancement at lower applied voltages than previously observed or predicted.

4.2 Materials and methods

4.2.1 Experiment design

The general design and fabrication of the device (Figure 4.1) consisted of a 20 μL glass plate inlet reservoir (9 mm × 6 mm × 365 μm) and 2 mL outlet vial fluidically connected using a 10 cm long fused silica capillary (75 μm i.d. 365 μm o.d., Polymicro Technologies, Phoenix, USA). An electrode was constructed exactly at the capillary channel entrance similar to Chapters 2 and 3 [15, 17].

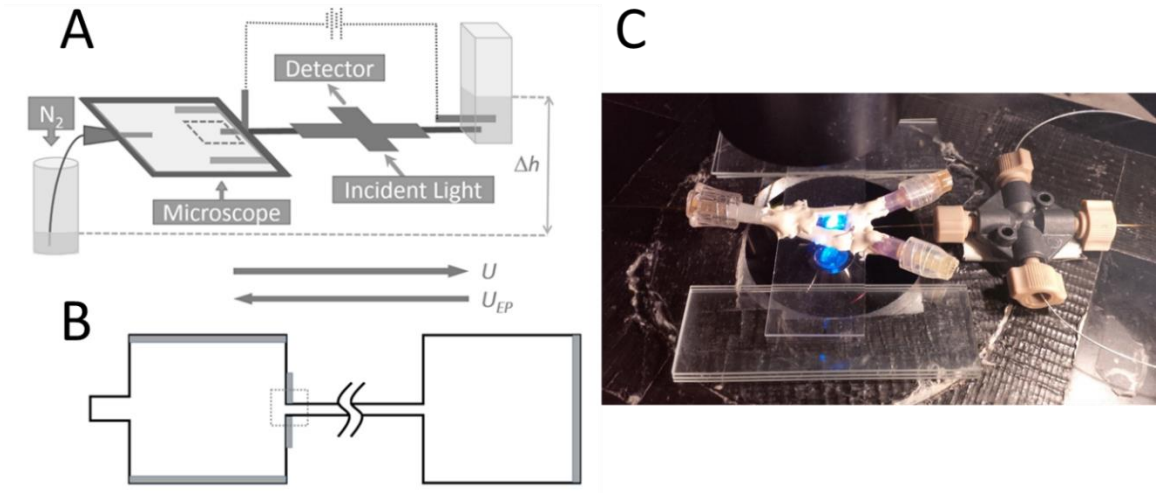

Figure 4.1. (A) Schematic of experimental design. A flat-glass plate reservoir (far left) above the microscope objective is filled by applying nitrogen gas to a sample feed reservoir. A capillary channel connects the plate reservoir, which serves as the inlet, and cuvette outlet reservoir (far right). Bulk fluid velocity (U) and direction were controlled by adjusting the gas and hydrostatic pressure (induced by the fluid level height difference (Δh) between the feed reservoir and outlet). EP velocity (U_{EP}) was controlled based upon electric field magnitude and analyte EP mobility. (B) Representative 2-D finite element analysis model with shaded lines representing boundary electrodes. Dashed boxes in A and B represent channel entrance regions of interest.

Fluid flow was controlled using both hydrostatics and house nitrogen. Setting the total pressure by countering one another allowed changes to flow magnitude and direction with simple adjustment of the nitrogen pressure, monitored with sensor (GPS-BTA, Vernier, Beaverton, USA), and/or vial height via bench-top scissor lift. Volume flow rate was calculated using density and weight of liquid collected from the channel during a set time and temperature, and then converted to average flow velocity. The velocities from each pressure source were tested independently by removing the other pressure source during measurement.

The bulk fluid utilized in the experiments was a 5 mM phosphate buffer (Sigma Aldrich, St. Louis, USA) with pH of 2.2. Rhodamine 123, a cationic fluorescent dye

(Molecular Probes, Grand Island, USA), was prepared at 5 µM for use in the concentration monitoring experiments. Prior to conducting experiments, the reservoirs and channels were preconditioned with buffer for a minimum of 30 minutes and then the rhodamine 123 was added and allowed to reach a steady state concentration throughout the system.

Concentration monitoring was accomplished using fluorescent microscopy at the channel entrance and on-capillary visible spectroscopy midway down the channel with setups similar to Chapters 3 and 4. An Ocean Optics USB 4000 visible spectrometer (Dunedin, USA) with optical fibers positioned perpendicular to and 5.2 cm down the channel was employed for the spectroscopic measurements.

4.2.2 Model design

A 2-dimensional finite elemental analysis model developed with COMSOL Multiphysics 4.4 software (COMSOL, Inc., Los Angeles, USA) was used to calculate the transport dynamics of the electrophoretic exclusion construct. The model geometry closely mirrored that of the fabricated device with the exception of the reservoir sizes and length of the feed reservoir tubing. To minimize unnecessary meshing, the model reservoir dimensions were reduced approximately 10-fold without causing a significant change to the overall hydraulic and ohmic resistances. The ~1000-fold reduction in the length of the model feed reservoir tubing was accounted for by using the software's built-in correction factor under the laminar flow interface where the length of the inlet channel outside the model domain can be defined (46 cm in this case). Liquid, silica glass, and copper materials were selected from the built-in library and assigned to the respective geometric entities. The liquid electrical conductivity was modified to reflect that of the

phosphate buffer used in the experiments. The laminar flow, electric current, and transport of dilute species interfaces were coupled during the simulations. Electric potential (800 V) was assigned to an electrode boundary located 1 mm from the exit in the reservoir, while ground was assigned to both the electrode boundary on the capillary face and to the electrode boundaries along the inlet reservoir edges parallel to the length of the capillary (Figure 4.1). All other boundaries were defined as electrical insulation. Laminar, incompressible flow was assigned to all domains and a no slip condition to all boundary walls. The inlet boundary condition was set to a laminar inflow entrance pressure of 2068 Pa and entrance length of 46 cm. The outlet boundary condition was set to a 1582 Pa no viscous stress pressure resulting in a net pressure of 486 Pa towards the outlet. Rhodamine 123 was assigned an initial concentration of 0.001 mol/m^3 for all domains and an EP mobility of 1.8×10^{-8} $m^2/(Vs)$, determined experimentally using traditional CE with similar concentration and buffer composition. The quadratic shape function order within the *Transport of Diluted Species* interface was selected in place of the linear option to improve the accuracy of the results for low Reynolds number flow such as those in this model. A 5 µm wide and 75 µm high rectangular domain probe was inserted midway down the channel simulating a spectroscopic detection zone for monitoring local average concentration. All other model parameters were left at default and, where applicable, closely mirrored the fabricated device and experimental conditions.

4.3 Results and discussion

4.3.1 Simulation demonstrating localized exclusion and concentration enhancement

A simulation was performed to first assess the lateral fluid velocity field within the channel entrance region. Given the low Reynolds number for this system, the characteristic features of laminar flow were assumed within the channel. Here, fully developed flow, or the lack of a longitudinal gradient, results along all laminae a few microns inside the channel. The maximum velocity lamina (U_{max}) resides at the longitudinal centerline and the effective (sometimes "average") velocity lamina (U_{eff}) = ½*(U_{max}), resides parallel to and between U_{max} and the channel wall, where U_{wall} = 0 μm/s. The simulation was consistent with the laminar flow description evidenced by U_{max} residing along the centerline and decreased velocities along laminae nearer the wall (Figure 4.2A).

A simulation was also used to assess the lateral electric field within the channel entrance region. The electric field gradient remained largely unchanged from beyond 50 μm outside and 50 μm inside the entrance regardless of proximity to the channel wall (Figure 4.2B). However, a pronounced, non-uniform gradient resulted near the entrance along the cutline nearest the wall. The localized electric field spike as predicted by the simulation had twice the magnitude of the global electric field making it a potentially important feature within the electrophoretic exclusion construct.

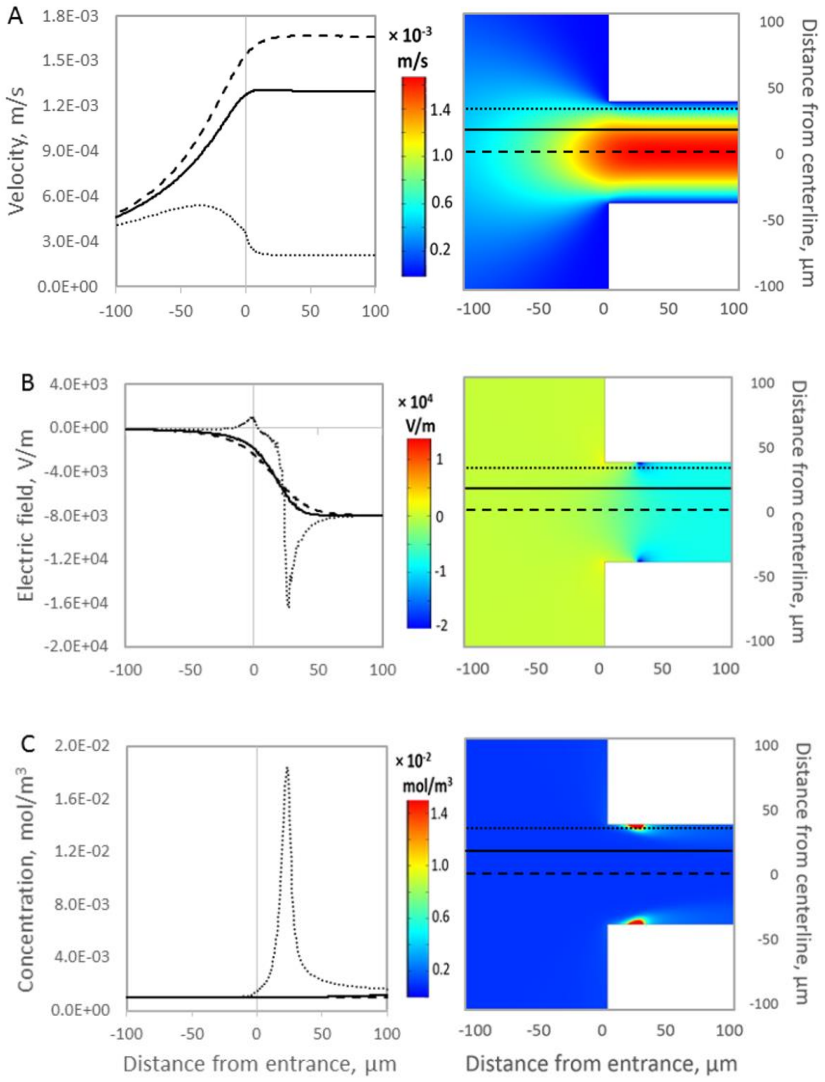

Figure 4.2. Flow velocity magnitude (A), electric field magnitude (B), and rhodamine 123 concentration profiles (C) near capillary entrance (x = 0) calculated from finite element simulation. Note patterned lines (each 17.5 µm apart) in right panels with corresponding univariate plots in the left panels. The combination of velocity and electric field lateral asymmetries create a concentration bolus (C) along the wall near the entrance.

The features of the independent flow and electric field calculations resulted in a prediction of a local increased concentration not noted in previous assessments (Figure 4.2C). Although the global pressure and electric field settings do not suggest the formation of a bolus under these conditions, the combination of localized velocity

minimums and electric field maximums near the entrance wall gave rise to a noticeable concentration enhancement near the corners.

The simulations can be presented such that experimental data can be directly compared to the results. Simulated time-dependent surface plot concentrations during applied potential and upon potential removal provided a visual and spectroscopic-like means to monitor concentration changes (Figure 4.3). Transport dynamics from diffusion, convection, and electrokinetic dispersion were included in the simulation to more closely match the conditions with which experimental data were collected.

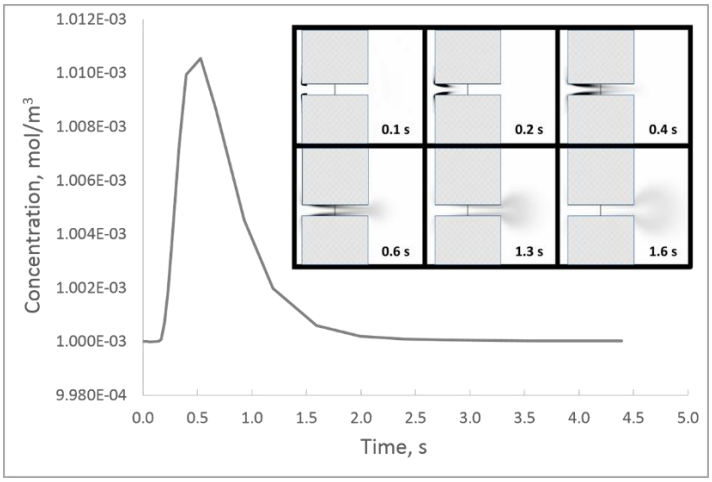

Figure 4.3. (Inset) Surface concentration plot from finite element simulation with voltage on (0.1 s) and immediately after it was removed (subsequent panels starting from middle top moving to bottom right). (One dimensional line plot) Concentration plot after potential was removed as detected midway down the channel (detection location at vertical line across channel depicted on inset).

4.3.2 Flow velocity and model validation

Since flow and electric fields must be carefully controlled and the electric field can be trivially controlled via external power supply, establishing known and controllable magnitude of fluid velocities was necessary to properly assess the experimental results. Gravimetrically calculated average fluid velocities from both hydrostatic forces and nitrogen gas pressures were compared to the 2-D finite element computer simulations and

Poiseuille's law. As expected, the average velocities increased linearly with increased pressure (Figure 4). The calculated and simulated values fell within the standard error of the experimentally determined values indicating reliable use of the simulation, fluid level height difference, and nitrogen pressure sensor as accurate and precise predictors of fluid velocity.

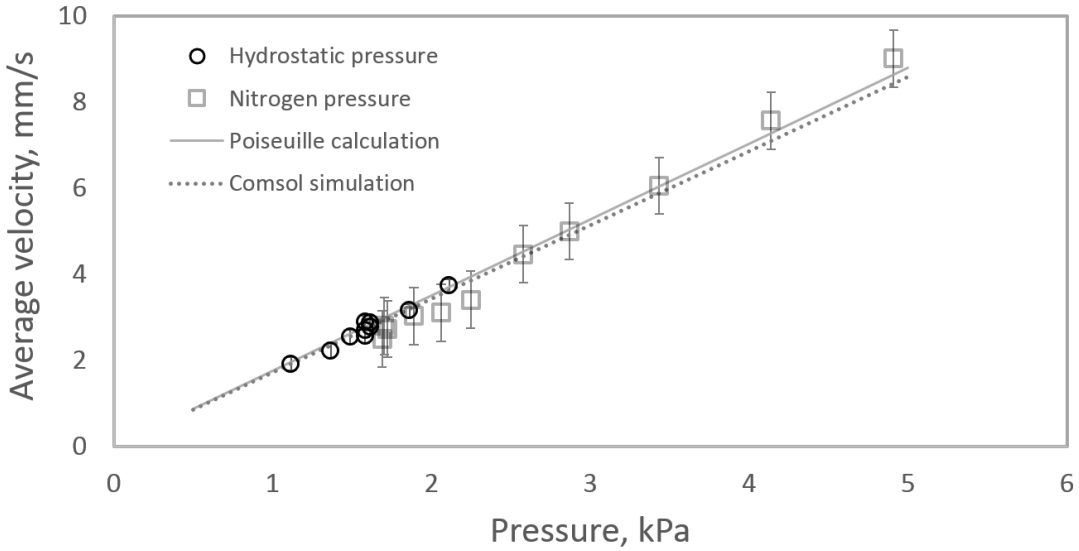

Figure 4.4. Comparison of calculated and measured fluid velocity. Average fluid velocity determined by fluid volume weight at various pressures induced by hydrostatic effects (circle markers) and nitrogen gas (square markers). Theoretical estimates of the system: Poiseuille's law (solid line) and model simulation (dashed line) for comparison.

Some assessment of the electric field can be made. The simulated electric field was compared to values according to a simple Ohmic model. The field well within the length of the capillary is estimated to be constant (E_{global}), according to $E_{global} = V / L$, where V is applied voltage, and L is channel length. Within the simulation, inputs of 800 V across the 10 cm channel generated a global electric field solution of 8000 V/m (Figure 4.2), which was consistent with the Ohmic result. Although the global electric field was not measured experimentally due to the device design prohibiting sample plug injection,

the agreement between the monitored current, Ohmic model, and the 2-D simulation supported the validity of the 2-D model.

4.3.3 Experiment demonstrating local exclusion and concentration enhancement

A local concentrated bolus is predicted by the simulations at a location that is difficult to image. Two temporal methods were used to confirm (or refute) the presence of a bolus under conditions where previous assessments suggest none should form. The examination of the simulation cutlines approaching the channel wall (Figure 4.2) exhibited varying localized velocity and electric field gradients relative to flat (non-gradient) global longitudinal velocity and global longitudinal and lateral electric fields found inside the channel. To determine whether these local gradients and their effects exist under experimental conditions, the concentration of rhodamine 123, a fluorescent and electrophoretically mobile dye, was monitored during conditions set similar to the simulation. While the lateral fields themselves cannot be directly visualized or assessed, monitoring the concentration at the entrance using fluorescent microscopy and midway down the channel with visible spectroscopy provided a means to test the model.

During the application of the same electric potential used in the simulation, no concentration increase was observed at the entrance area using the epifluorescent microscope. The simulation indicated that the concentrated zone resided just inside the channel as potential was applied and was consistent with no increase of fluorescence near the entrance (Figure 4.5A, first image on left). Figure 4.5A illustrates a 6.4 s montage of rhodamine 123 exiting the capillary after the local exclusion condition was established and subsequently pushed from the channel using reversed fluid flow so any local concentration enhancement could be visibly detected. The concentrated zone exiting the

channel in both the simulation and experiment contained higher concentrations on the periphery compared to the center (Figures 4.3A and 4.5A). A similar experiment was performed without changing flow direction or magnitude where the applied potential was removed to allow any collected sample to flow down the channel towards the spectroscopic detection zone (Figure 4.3B and 4.5B). Based on the bulk fluid velocity and the time to reach the detector, the original location of the concentrated zone was back-calculated to the channel entrance, consistent with the simulation results (Figure 4.3A). Similarities between the spectroscopic and simulated probe peak shapes (Figures 4.5B and 4.3B, respectively) as well as the consistent shape and general appearance between the concentration zones in both the microscope and simulation studies, further supported the notion that the localized lateral field effects observed during the simulation were also present in the experimental.

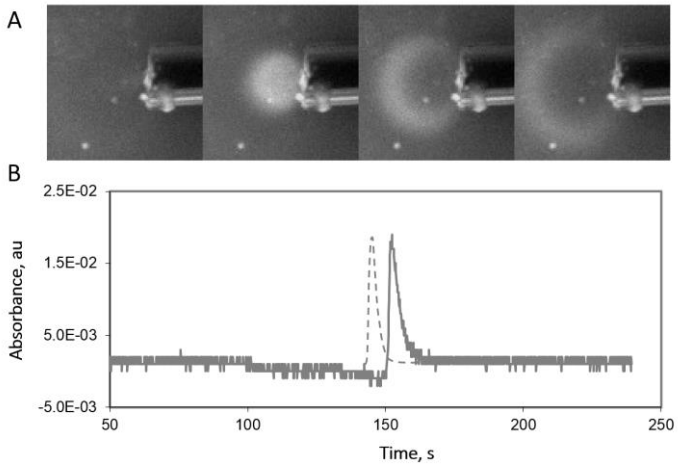

Figure 4.5. Images of dye dynamically exiting a capillary and plot of bolus passing a detector within the capillary. Rhodamine 123 exiting capillary entrance (A) after local exclusion and flow direction reversal. Capillary width = 360 µm, channel diameter = 75 µm, frame interval = 1.6 s. See Figure 1 Microscope for region of interest probed. Spectroscopic plot of Rhodamine 123 midway down channel (B) after a 60 s applied voltage was removed at 90 s. Plot shape is representative of other data sets collected under similar conditions. Dashed plot is a normalized overlay of model data from Figure 3B offset from this experimental data for comparison. See Figure 1 detector for region of interest probed.

Under normal exclusion conditions as demonstrated in previous works, where U_{EP} of the analyte meets or exceeds U_{eff} at steady state, complete analyte exclusion occurs and any analyte initially inside the channel prior to applied voltage is evacuated. However, under the conditions described in this work, where U_{EP} (calculated using the globally applied voltage) was five times less than U_{eff}, no exclusion or discernable concentration enhancement would be expected, especially with convective and diffusional dispersive forces inherent with the system. Instead, the coupling of the sudden decrease in fluid velocity with the sharp local electric field at the corner created a localized concentration bolus confined to the entrance corner region when voltage was applied.

With the characterization of both the longitudinal and lateral velocity and electric fields of the currently adopted EP exclusion design, strategic manipulation of the device geometry and electrode configuration can be considered for improved resolution and overall performance. One such non-trivial approach would be the suppression of any lateral gradient so an analyte approaching the channel entrance from any direction would be subject to only a single, well-defined, sharp longitudinal gradient for either the velocity or electric field components. Another attempt may instead be the manipulation of the geometry and electrodes of the current system to further exploit the corner gradient spikes generated at relatively low applied voltages. With either approach, the continued modeling and experimental testing of the field effects within the EP exclusion construct will play an important role for efficient device design.

4.4 Concluding remarks

To design a high resolution separation interface utilizing a punctuated electrophoretic counter-flow gradient approach like EP exclusion, the electric and velocity fields across the entire separation domain must be understood. This work demonstrated the relationship between localized asymmetric electric and velocity fields near a converging channel entrance and revealed their impact on the EP exclusion condition. With the goal of establishing a separation interface where analytes of a certain EP mobility do not enter the channel and simultaneously pre-concentrate relative to those of a slightly lower EP mobility that pass through the channel, the need to limit interfacial field gradient variations that directly influence analyte velocities, and consequently separation resolution, becomes apparent. The agreement between the experimental and simulation data from this study warrants future use of the simulation to explore how changes to device design parameters like entrance corners, channel diameter, and electrode configuration can impact resolution. Tailoring the device design to maximize resolution at a single interface will further support the feasibility of engineering high resolution parallel interfaces for separating and concentrating electrophoretic species from complex samples.

4.5 References

[1] Albin, M., Grossman, P. D., Moring, S. E. *Anal. Chem.* 1993, *65*, 489A-497A.

[2] Lian, D., Zhao, S., Li, J., Li, B. *Analytical and bioanalytical chemistry* 2014, *406*, 6129-6150.

[3] Dawod, M., Chung, D. S. *Journal of Separation Science* 2011, *34*, 2790-2799.

[4] Breadmore, M. C., Shallan, A. I., Rabanes, H. R., Gstoettenmayr, D. *et al*. *Electrophoresis* 2013, *34*, 29-54.

[5] Chiu, T. *Analytical and Bioanalytical Chemistry* 2013, *405*, 7919-7930.

[6] Kitagawa, F., Otsuka, K. *Journal of Chromatography A* 2014, *1335*, 43-60.

[7] Chien, R. *Electrophoresis* 2003, *24*, 486-497.

[8] Wang, C., Her, G. *Electrophoresis* 2014, *35*, 1251-1258.

[9] Mikkers, F. E. P., Everaerts, F. M., Verheggen, T. P. E. M. *Journal of Chromatography A* 1979, *169*, 1-10.

[10] Burgi, D. S., Chien, R. L. *Anal. Chem.* 1991, *63*, 2042-2047.

[11] Simpson, J.,Steven L., Quirino, J. P., Terabe, S. *Journal of chromatography.A* 2008, *1184*, 504-541.

[12] Giddings, J. C., Dahlgren, K. *Separation Science* 1971, *6*, 345-356.

[13] Meighan, M. M., Staton, S. J., Hayes, M. A. *Electrophoresis* 2009, *30*, 852-865.

[14] Shackman, J. G., Ross, D. *Electrophoresis* 2007, *28*, 556-571.

[15] Polson, N. A., Savin, D. P., Hayes, M. A. *J. Microcolumn Sep.* 2000, *12*, 98-106.

[16] Pacheco, J. R., Chen, K. P., Hayes, M. A. *Electrophoresis* 2007, *28*, 1027-1035.

[17] Meighan, M. M., Keebaugh, M. W., Quihuis, A. M., Kenyon, S. M., Hayes, M. A. *Electrophoresis* 2009, *30*, 3786-3792.

[18] Kenyon, S. M., Keebaugh, M. W., Hayes, M. A. *Electrophoresis* 2014, *35*, 2551-2559.

[19] Sikorsky, A. A., Fourkas, J. T., Ross, D. *Anal. Chem.* 2014, *86*, 3625-3632.

[20] Keebaugh, M. W., Mahanti, P., Hayes, M. A. *Electrophoresis* 2012, *33*, 1924-1930.

[21] Kenyon, S. M., Weiss, N. G., Hayes, M. A. *Electrophoresis* 2012, *33*, 1227-1235.

Chapter 5

Initial optimization of electrophoretic exclusion

5.1 Introduction

A benchmark for defining the success of an analytical separation is whether it has adequate resolution to segregate one sample component from another. Some of the more traditional and well-established separation techniques like chromatography [1, 2] and capillary electrophoresis (CE) [3] have theoretically derived and experimentally validated methods to assess resolution Equilibrium gradient separation techniques, known for simultaneous separation, concentration enhancement, and decreased dispersion, have a theoretical resolution construct described by Giddings *et al*. [4]. Novel separation techniques based on the general equilibrium gradient approach often require a modified theoretical framework to accurately predict resolution for the specific system [5]. Electric field gradient focusing (EFGF) resolution has been described by comparing the focusing effects near the equilibrium point to that of a spring using Hooke's law [6]. Likewise, a theoretical resolution framework for gradient elution moving boundary electrophoresis (GEMBE), another equilibrium gradient method, was developed to allow a direct comparison to CE [7].

Electrophoretic exclusion is a technique with similar equilibrium gradient characteristics as EFGF except instead of posing hydrodynamic flow against an electrophoretic velocity gradient inside the channel, the equilibrium gradient condition is initiated directly at the channel entrance so as to create a differentiation zone where substances either enter the channel or are excluded based on their physical properties. The localized microgradient initiated at the electrode/solution interface and the lack of

traditionally formed chromatographic peaks under ideal conditions prevent a direct translation of EFGF resolution theory to this technique. Preliminary success of electrophoretic exclusion had been demonstrated experimentally for a variety of analytes [8-10] and theoretically using modeling and simulation. While the results from these studies helped establish threshold values, quantify velocity and electric field magnitudes [11], and provided a detailed visualization of opposing field effects at the exclusion entrance [12], they did not result in the ability to predict the resolving power of electrophoretic exclusion.

A thorough study of the resolution capabilities of electrophoretic exclusion from a traditional separations science point-of-view was conducted by Kenyon *et al*. [13]. In this theoretical assessment, resolution was defined using common dimensionalities, materials, and electric potential magnitudes created at a straight channel interface with integrated electrode. This theory provided a foundational framework to interrogate the resolving power of electrophoretic exclusion.

The aim of this work is to assess the resolution of the electrophoretic exclusion design described above and in Chapters 2-4 both experimentally and with the use of modeling. Electrophoretic exclusion resolution theory is briefly defined to establish key terms and variables and the resulting theoretical resolution is compared to existing techniques. A mixture of Rhodamine 6G and rhodamine B is used to evaluate the resolving power of the current device design. A method to assess resolution within the simulation construct is developed so that the calculations can be compared to the experimental results and theoretical predictions. Simulation resolution predictions are in general agreement with early experimental assessments, both suggesting species with

electrophoretic mobilities as similar as 10^{-9} $m^2/(Vs)$ can be separated with the current design. Resolution interrogation from both a theoretical assessment and simulation construct demonstrate resolution improvement with decreased channel width and placement of an electrode directly at the interface. Results provide a proof-of-concept for using the model as an accurate tool to assess resolution so that different device designs can be quickly modeled and compared for optimizing electrophoretic exclusion performance.

5.2 Theory

The degree of separation, or resolution (R), of two adjacent analyte bands is commonly defined as the distance between band centers (ΔX) divided by the average band width, which can be expressed using the standard deviation of the distribution of those bands (σ) (Figure 5.1) [14].

$$R = \frac{\Delta X}{4\sigma} \tag{5.1}$$

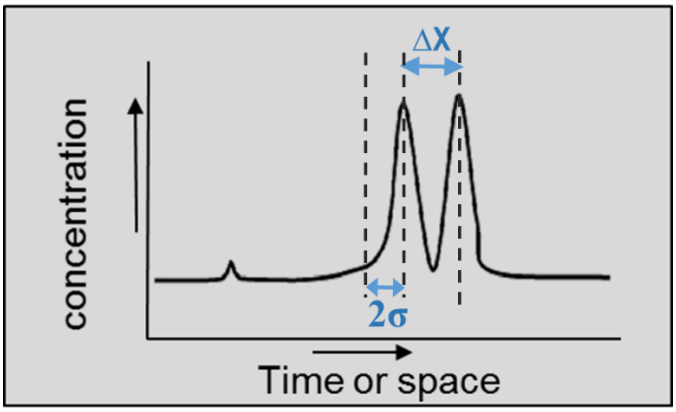

Figure 5.1. Depiction of typical chromatographic resolution.

The larger the R, the greater the disengagement of the two bands; R = 1 corresponds to a reasonably good separation and R = 1.5 corresponds to the complete separation of the

two bands (so-called *baseline separation*) [15]. For traditional techniques, the parameters ΔX and σ are easily defined. However, electrophoretic exclusion does not produce traditional concentration bands and the distance between two separated bands cannot be defined in the traditional sense. Instead, a new framework, briefly described below, was created using foundational principles to define the resolution at the separation interface [13].

The assessment of the width of the exclusion zone was approximated using an error function to describe the steady state separation condition where the dispersion forces are equivalent and opposite the flow and electrophoretic forces [16]. The variance (σ^2) associated with the error function included all dispersive forces (D_{TOT}) competing with the restorative forces similar to equilibrium gradient steady state methods described in Giddings [4].

$$\sigma^2 = \frac{D_{TOT}}{change\ in\ velocity\ with\ position} \tag{5.2}$$

The total dispersive forces causing band broadening included diffusion (D_{diff}) and Taylor-Aris dispersion, which is dependent on flow velocity (v) and channel diameter (d) [17].

$$D_{TOT} = D_{diff} + \frac{v^2 d^2}{192 D_{diff}} \tag{5.3}$$

The *change in velocity with position* described the electrophoretic focusing effects across the interface and was dependent on both the field gradient *dE/dx* at the entrance and the average electrophoretic mobility (μ_{ave}) between two arbitrarily closely related species, resulting in a variance:

$$\sigma^2 = \frac{D_{diff} + \frac{v^2 d^2}{192 D_{diff}}}{\mu_{ave} \frac{dE}{dx}} \tag{5.4}$$

and standard deviation:

$$\sigma = \sqrt{\frac{D_{diff}+\frac{v^2 d^2}{192 D_{diff}}}{\mu_{ave}\frac{dE}{dx}}} \tag{5.5}$$

Without defined bands as in traditional separations, determining the distance between bands (ΔX) was not possible with electrophoretic exclusion. Instead, ΔX was defined as a function of the electric field difference between two nearest neighbor channel entrances in a serial channel configuration. With this construct, the gradient transition between the channel entrances was related to the distance between the channels. The sharper the transition (proportional to *dE/dx*), the closer the channels could be relative to one another (proportional to ΔX), giving:

$$\Delta X = \frac{\Delta \mu E_{ave}}{\frac{1}{2}\mu_{ave}(\Delta\frac{dE}{dx})} \tag{5.6}$$

Resolution could then be described by:

$$R = \frac{\Delta X}{4\sigma} = \frac{\Delta \mu E_{ave}\sqrt{\frac{dE}{dx}}}{2\sqrt{\mu_{ave}}\Delta\frac{dE}{dx}\sqrt{D_{diff}+\frac{v^2 d^2}{192 D_{diff}}}} \tag{5.7}$$

Determining the two closest resolvable species, or the smallest change in electrophoretic mobilities, could be assessed by solving the resolution for $\Delta\mu$, where R = 1.5.

$$\Delta\mu_{min} = \frac{3\sqrt{\mu_{ave}}\Delta\frac{dE}{dx}\sqrt{D_{diff}+\frac{v^2 d^2}{192 D_{diff}}}}{E_{ave}\sqrt{\frac{dE}{dx}}} \tag{5.8}$$

5.3 Materials and Methods

5.3.1 Model development

To assess the theoretical resolution of different interface designs, two-dimensional electrophoretic exclusion models similar to those which have been experimentally validated were used [11]. These models utilized finite element analysis within COMSOL Multiphysics 5.1 software (COMSOL, Inc., Los Angeles, USA). The software physics interfaces simulated the electric field (using Ohm's law and Gauss' law), laminar flow (using Navier-Stokes equation), and molecular transport, which included diffusion (using Fick's law), convective dispersion (using diffusion coupled with a velocity vector), and electrophoretic migration transport (using diffusion coupled with Ohm's law for ionic current transport). The coupling of these physics interfaces enabled concentration monitoring of charged species during electrophoretic exclusion and a method to assess resolution.

The model geometry consisted of two 1.5 mm × 3.0 mm rectangular reservoirs connected by a 1 mm long channel of varying widths. Liquid, silica glass, and copper materials were selected from the built-in library and assigned to the respective geometric entities. Electric potential (75 V when applied) was assigned to the electrode boundary in the exit reservoir, and ground was assigned to the capillary face and inlet reservoir edge boundaries as in Chapter 4. All other boundaries were defined as electrical insulation. Laminar, incompressible flow was assigned to all domains and a no slip condition to all boundary walls, unless otherwise noted. The laminar inflow boundary on the reservoir edge was set to an average velocity of 5 μm/s providing a 1.4 mm/s fully developed centerline velocity in the channel entrance. This centerline velocity was maintained

between trials involving different channel widths by varying the velocity inflow. The outlet boundary pressure on the exit reservoir edge was set to 0 Pa.

Six dependent variables representing six different analytes were added to the *transport of dilute species* interface. These analytes were assigned identical initial molar concentrations and identical diffusion coefficients but unique electrophoretic mobilities. The quadratic shape function order within the *transport of dilute species* interface was selected in place of the linear option to improve the accuracy of the results for low Reynolds number flow such as those in this model.

5.3.2 Experimental conditions

The electrophoretic exclusion device and experimental setup used to assess resolution were the same as those described in Chapter 4. Similarly, the bulk fluid was a 5 mM phosphate buffer (Sigma Aldrich, St. Louis, USA) with pH of 2.2. Rhodamine 6G (Molecular Probes, Grand Island, USA) and rhodamine B (Aldrich Chemical Company, Milwaukee, USA) both cationic fluorescent dyes, were prepared at 5 μM with the phosphate buffer. Concentrated hydrochloric acid (HCl, EMD, Savannah, GA) was diluted to 0.1M with 18 MΩ water for device preconditioning.

5.4 Results and Discussion

5.4.1 Comparison of electrophoretic exclusion theory to other techniques

Electrophoretic exclusion, in the general sense, does not produce traditional chromatographic or electrophoretic peaks of a defined width separated by a specified time or space. Rather, the interface properties inherent with this technique provide separation by either excluding analytes from entering the channel or allowing them to enter and pass through. To assess and compare the theoretical performance of this

technique directly with the performance of other separation techniques or device designs, the value of $\Delta\mu_{min}$, or the minimum resolvable electrophoretic mobility difference between two species, was used [13]. With this assessment the smaller the value of $\Delta\mu_{min}$, the better the resolution for the given technique.

According to the calculations presented in Kenyon *et al*, $\Delta\mu_{min}$ (R = 1.5) $\approx 10^{-12}$ $m^2V^{-1}s^{-1}$ for electrophoretic exclusion, where the capillary diameter was equal to 20 µm, the electric field was set at 5×10^4 V/m, the flow rate was 20 nL/min, the diffusion coefficient was 6×10^{-8} m^2s^{-1}, and μ_{ave} was 5.0×10^{-9} m^2 $V^{-1}s^{-1}$ [13]. Compared to the other electrophoretic techniques summarized in Table 5.1, the theoretical resolution of electrophoretic exclusion was on par with some of the best resolution techniques.

Table 5.1. Summary of best resolution (smallest $\Delta\mu_{min}$) for different electrophoretic separation techniques [7, 13, 18, 19]

$\Delta\mu_{min}$ $(m^2/(Vs))$	Electrophoretic Method	Reference
10^{-10}	Capillary Zone Electrophoresis (CZE)	Culbertson, C. T., Jorgenson, J. W. *Anal. Chem.* 1994, *66*, 955-962.
10^{-11}	Flow Counterbalanced CE	Culbertson, C. T., Jorgenson, J. W. *Anal. Chem.* 1994, *66*, 955-962.
10^{-12}	Ultra-high Voltage CZE	Hutterer, K., Jorgenson, J. *Anal. Chem.* 1999, *71*, 1293-1297.
10^{-9}	Gradient Elution Moving Boundary Electrophoresis (GEMBE)	Ross, D. *Electrophoresis* 2010, *31*, 3650-3657.
10^{-12}	Electrophoretic Exclusion Theory	Kenyon, S. M., Keebaugh, M. W., Hayes, M. A. *Electrophoresis* 2014, *35*, 2551-2559.

5.4.2 Experimental assessment of electrophoretic exclusion resolution

A preliminary assessment of electrophoretic exclusion resolution could be made using experimental data obtained in previous studies. Rhodamine 6G and rhodamine B, each with distinct electrophoretic mobility, were combined and introduced into the device

shown in Figure 4.1 to determine if the more mobile species, rhodamine 6G in this case, could be differentially excluded from rhodamine B. The flow injection spectroscopic plots of both dyes after an exclusion condition was initiated (Figure 5.3) illustrated that both dyes were at least partially excluded. This indicated that $\Delta\mu_{min}$ for this particular experiment was no less than 2×10^{-9} $m^2/(Vs)$, and slightly worse than the 10^{-11} $m^2/(Vs)$ value predicted by equation 5.8. An independent but comparable study also obtained a $\Delta\mu_{min}$ value on the order of 10^{-9} $m^2/(Vs)$) [9]. Both studies employed an indirect flow injection analysis method that may have contributed to the value discrepancy. Additionally, the lateral field asymmetries described in Chapter 4 that can cause localized concentration build-up may have a limiting effect on maximizing the resolution of the 75 μm diameter capillary device design. In fact, direct observations of fluorescent dye at the interface of a planar microfluidic chip demonstrated very sharp concentration gradients less than 100 μm indicating the experimental flow and electric field effects were consistent with the theoretical model, further suggesting that the 75 μm diameter capillary interfaces were not optimized for resolution [8].

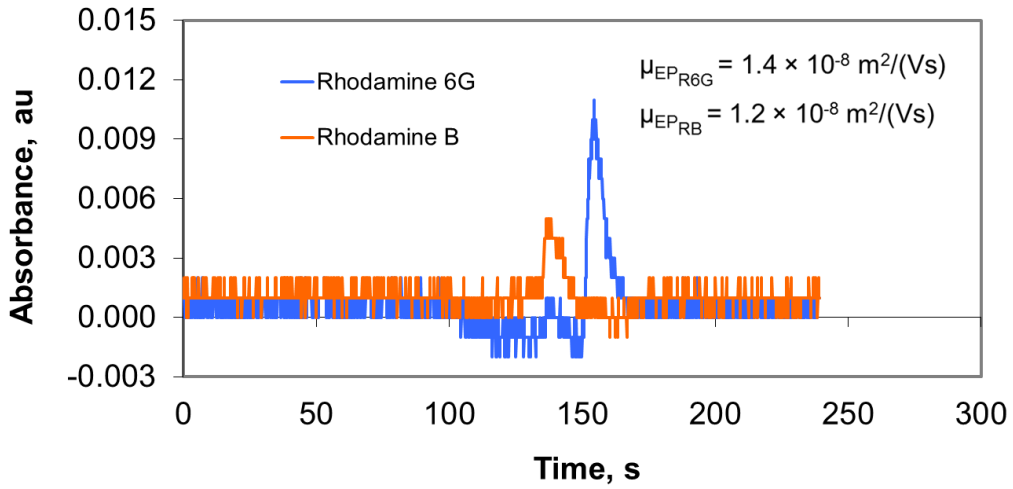

Figure 5.2. Flow injection analysis of rhodamine 6G and rhodamine B. The two dyes were not fully resolved (one excluded and one not) indicating $\Delta\mu_{min}$ was no less than 2 × 10^{-9} m^2/(Vs), determined by the difference in displayed electrophoretic mobilities.

5.4.3 Construct to assess exclusion using model

Evaluation of the model resolution involved monitoring the concentrations of six analytes with distinct electrophoretic mobilities to determine the smallest change in electrophoretic mobilities ($\Delta\mu_{min}$) that could be fully resolved, or in this case excluded versus not excluded (see Figure 1.7C for illustration of $\Delta\mu_{min}$). To monitor concentration over time, a rectangular domain probe with a length of 50 μm and width equal to the channel diameter was inserted midway down the channel simulating a spectroscopic detection zone for monitoring local average concentration. The placement of this detection zone was such that it was removed from the interface region where varying gradients and localized concentration effects can occur (Chapter 4), and instead was located in a region where the velocity and electric fields were fully developed in order to achieve the most accurate assessment of the analytes' movement through, or exclusion from, the channel.

Of the six analytes arbitrarily labeled *A* through *F*, analyte *A* was assigned an electrophoretic mobility of 0 $m^2/(Vs)$ to serve as a neutral control during the simulation. This ensured the time-dependent simulation was run long enough for the inflowing analytes to reach the detection zone, and it provided a baseline concentration (C_o) at the detection zone to which the non-neutral analyte concentrations (*B*-*F*) could be normalized (Figure 5.2). Full exclusion, or 100% exclusion, occurred when a non-neutral analyte was prevented from reaching the detection zone. No exclusion, or 0% exclusion, occurred when the concentration of a non-neutral analyte equaled or exceeded the concentration of *A* at the detection zone. Partial exclusion occurred when some (> 0% but < 100%) of the non-neutral analyte reached the detection zone. The value of $\Delta\mu_{min}$ was calculated by finding the difference between the largest electrophoretic mobility exhibiting 0% exclusion and the smallest electrophoretic mobility exhibiting 100% exclusion.

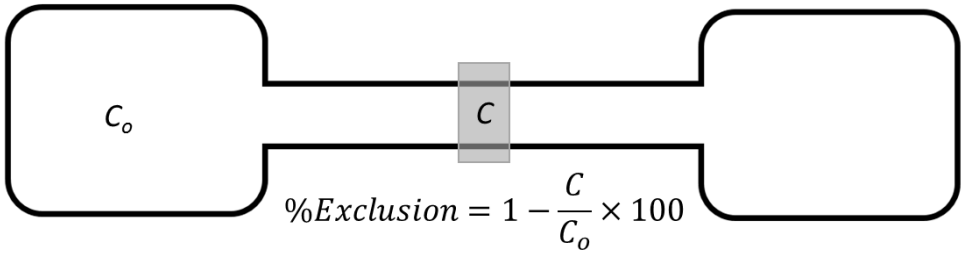

Figure 5.3. Construct to evaluate resolution of various interface designs.

5.4.4 Interface optimization: Channel diameter and flow rate

According to the electrophoretic exclusion model and its theoretical assessment, several parameters influence resolution. These are capillary diameter, flow rate, average electrophoretic mobility, field strength inside the channel, and the difference in field strength between adjoining entrances.

The relationship between resolution, channel diameter, and flow rate according to equation 5.8 were assessed graphically (Figure 5.4). Here, $\Delta\mu_{min}$ was minimized for small diameters and low flow rates. The smaller channel diameters positively influenced resolution through two mechanisms - increased electric field gradient and reduced Taylor-Aris dispersion - explaining why changing diameter is presumed to have a more dramatic effect on resolution as depicted in Figure 5.4 [13].

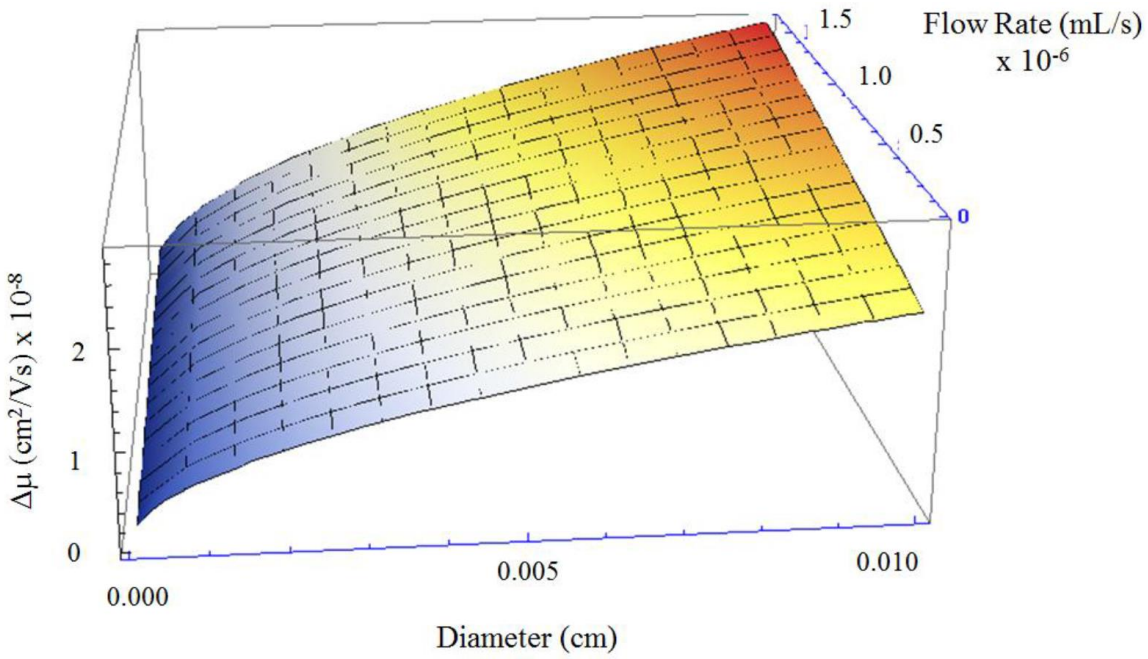

Figure 5.4. Resolution ($\Delta\mu$) as a function of capillary diameter and flow rate.

Assessment of resolution as a function of channel diameter was also performed using simulation. The construct describe in section 5.4.4 was used to evaluate the simulated transport of several species, each with a slightly different electrophoretic mobility, to determine which species were fully excluded versus not at all. Figure 5.5 provides a graphical summary of how close two species' electrophoretic mobilities can be to one another ($\Delta\mu_{min}$; *x*-axis) while still being segregated (one species undergoes 0%

exclusion, the other is 100% excluded). The steeper the plot slope, the smaller the $\Delta\mu_{min}$ and better the resolution. For three different channel widths (15 µm, 75 µm, 105 µm), the simulation predicted that smaller channel diameters will provide better resolution, which was in agreement with the theoretical prediction (Figure 5.3).

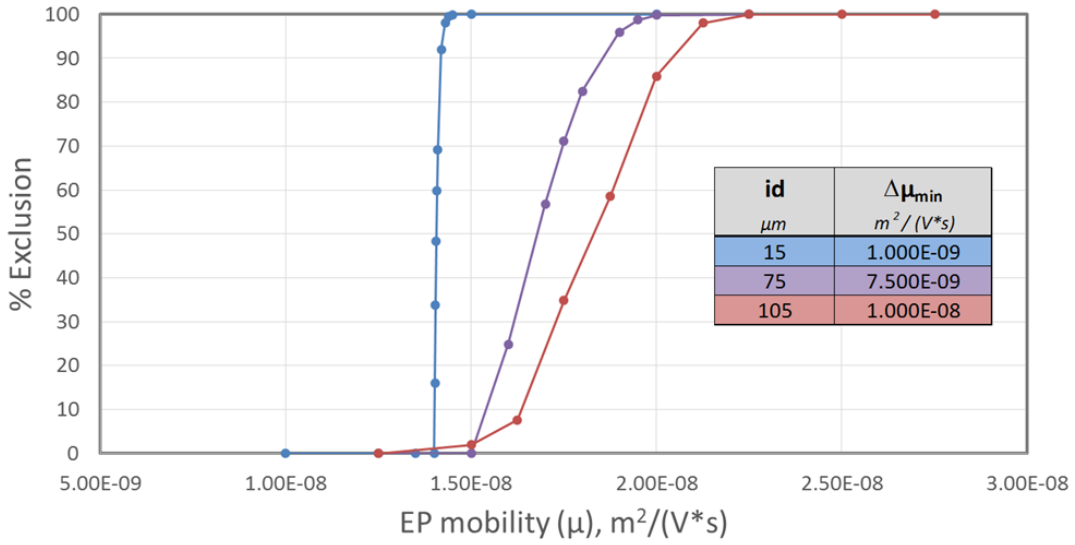

Figure 5.5. Electrophoretic exclusion performance as a function of channel inner diameter (id). The steeper the slope, the better the resolution.

5.4.5 Interface optimization: Electric field gradient

Assessment of resolution as a function of interface electric field gradient was also performed using simulation. Equation 5.8 indicated that a sharper electric field gradient at the entrance will result in a smaller $\Delta\mu_{min}$. Since the electric field gradient is directly tied to the channel diameter, two channels of equal diameter were used. The results of the simulation are depicted in Figure 5.5 and demonstrate the dramatic effect that the electric field at the interface can have on system performance. While these simulation results also agree with the theoretical framework, they also highlight the possibility of using different electrode configurations to shape the interfacial fields to improve resolution.

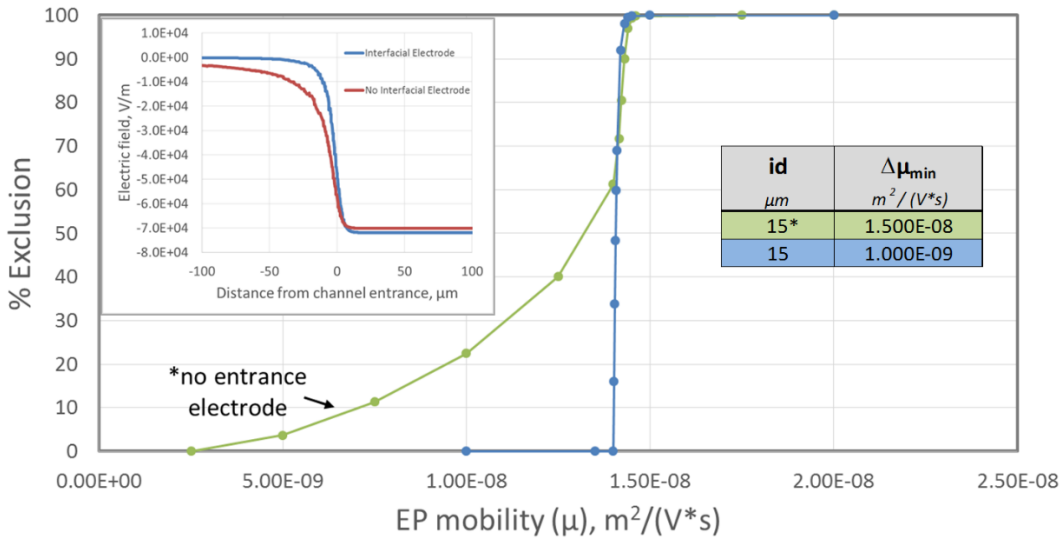

Figure 5.6. Electrophoretic exclusion performance as a function of electric field gradient. The steeper the plot slope, the better the resolution. The inset depicts the centerline electric field magnitude at the entrance with an interfacial electrode (blue plot) and without an interfacial electrode (red plot). The steeper the electric field gradient, the better the resolution.

5.5 Concluding remarks

Using an experimentally validated model to evaluate resolution can provide a fast, cheap, and reliable method to explore various interface designs for optimization. Results from Chapters 2, 3, 4, and 5 pointed to the strong possibility that lateral, or corner, gradient effects present themselves within the current device design and that these localized effects may have a negative impact on resolution. This was further supported by the inability to fully resolve rhodamine 6G from rhodamine B. The development of a construct to evaluate the impacts of various changes to device design and their effects on resolution was presented. Results demonstrated the strong resolution dependency on interface diameter and electrode placement as predicted by the resolution theory and serving as a proof-of-concept for the evaluation construct. The use of the simulation to

assess device resolution as a function of changing parameters can be expanded to assess other parameters about this interfacial region in an effort to develop a more optimized exclusion zone.

5.6 References

[1] Giddings, J. C. *J. Chromatogr.* 1960, *3*, 520-523.

[2] Giddings, J. C. *Anal. Chem.* 1963, *35*, 2215-&.

[3] Foret, F., Deml, M., Bocek, P. *J. Chromatogr.* 1988, *452*, 601-613.

[4] Giddings, J. C., Dahlgren, K. *Separation Science* 1971, *6*, 345-356.

[5] Tolley, H. D., Wang, Q. G., LeFebre, D. A., Lee, M. L. *Anal. Chem.* 2002, *74*, 4456-4463.

[6] Kelly, R. T., Woolley, A. T. *Journal of Separation Science* 2005, *28*, 1985-1993.

[7] Ross, D. *Electrophoresis* 2010, *31*, 3650-3657.

[8] Kenyon, S. M., Weiss, N. G., Hayes, M. A. *Electrophoresis* 2012, *33*, 1227-1235.

[9] Meighan, M. M., Keebaugh, M. W., Quihuis, A. M., Kenyon, S. M., Hayes, M. A. *Electrophoresis* 2009, *30*, 3786-3792.

[10] Meighan, M. M., Vasquez, J., Dziubcynski, L., Hews, S., Hayes, M. A. *Anal. Chem.* 2011, *83*, 368-373.

[11] Keebaugh, M. W., Mahanti, P., Hayes, M. A. *Electrophoresis* 2012, *33*, 1924-1930.

[12] Pacheco, J. R., Chen, K. P., Hayes, M. A. *Electrophoresis* 2007, *28*, 1027-1035.

[13] Kenyon, S. M., Keebaugh, M. W., Hayes, M. A. *Electrophoresis* 2014, *35*, 2551-2559.

[14] Giddings, J. C. *Unified separation science*, New York, Wiley 1991.

[15] Karger, B. L., Snyder, L. R., Horváth, C. *An introduction to separation science*, New York, Wiley 1973.

[16] Giddings, J. C. *Sep. Sci. Technol.* 1979, *14*, 871-882.

[17] Taylor, G. *Proceedings of the Royal Society of London Series A-Mathematical and Physical Sciences* 1953, *219*, 186-203.

[18] Culbertson, C. T., Jorgenson, J. W. *Anal. Chem.* 1994, *66*, 955-962.

[19] Hutterer, K., Jorgenson, J. *Anal. Chem.* 1999, *71*, 1293-1297.

Chapter 6

Concluding remarks

6.1 Electrophoretic Exclusion

Electrophoretic exclusion is a non-standard method of separation that according to initial theoretical resolution calculations, has the capability of high resolution interfacial segregation of components so long as the local electric field gradient remains high. The investigation of electrophoretic separation presented here has helped evolve the understanding of the interface region and built the foundation for exploring alternative device designs. The shaping of the channel entrance geometry and deliberate placement of electrodes about the entrance will positively influence the resolution of electrophoretic exclusion helping to fulfill integration into parallel configurations for multiplexed separations of complex samples.

REFERENCES

CHAPTER 1

[1] Kler, P. A., Sydes, D., Huhn, C. *Anal. Bioanal. Chem.* 2015, *407*, 119-138.

[2] Iliuk, A. B., Arrington, J. V., Tao, W. A. *Electrophoresis* 2014, *35*, 3430-3440.

[3] El-Baba, T. J., Lutomski, C. A., Wang, B., Inutan, E. D., Trimpin, S. *Anal. Bioanal. Chem.* 2014, *406*, 4053-4061.

[4] Giddings, J. C. *Unified separation science*, New York, Wiley 1991.

[5] Karger, B. L., Snyder, L. R., Horváth, C. *An introduction to separation science*, New York, Wiley 1973.

[6] Macášek, F., Navratil, J. D. *Separation chemistry*, New York, Ellis Horwood 1992.

[7] Zhao, S. S., Zhong, X., Tie, C., Chen, D. D. Y. *Proteomics* 2012, *12*, 2991-3012.

[8] Albalat, A., Mischak, H., Mullen, W. *Expert Review of Proteomics* 2011, *8*, 615-629.

[9] Rodriguez Robledo, V., Smyth, W. F. *Electrophoresis* 2014, *35*, 2292-2308.

[10] Kolch, W., Neusüß, C., Pelzing, M., Mischak, H. *Mass Spectrom. Rev.* 2005, *24*, 959-977.

[11] Jorgenson, J., Lukacs, K. *Science* 1983, *222*, 266-272.

[12] Issaq, H. *Electrophoresis* 1999, *20*, 3190-3202.

[13] Jorgenson, J., Lukacs, K. *J. Chromatogr.* 1981, *218*, 209-216.

[14] Jorgenson, J., Lukacs, K. *Anal. Chem.* 1981, *53*, 1298-1302.

[15] Kuehnbaum, N. L., Britz-McKibbin, P. *Chem. Rev.* 2013, *113*, 2437-2468.

[16] Giddings, J. C., Dahlgren, K. *Separation Science* 1971, *6*, 345-356.

[17] Wang, Q., Tolley, H., LeFebre, D., Lee, M. *Anal. Bioanal. Chem.* 2002, *373*, 125-135.

[18] Ista, L., Lopez, G., Ivory, C., Ortiz, M. *et al*. *Lab on a Chip* 2003, *3*, 266-272.

[19] Righetti, P. G., Drysdale, J. W. *Isoelectric focusing*, Amsterdam, North-Holland Pub. Co. 1976.

[20] Shackman, J. G., Ross, D. *Electrophoresis* 2007, *28*, 556-571.

[21] Ofarrell, P. H. *Science* 1985, *227*, 1586-1589.

[22] Greenlee, R. D., Ivory, C. F. *Biotechnol. Prog.* 1998, *14*, 300-309.

[23] Koegler, W. S., Ivory, C. F. *Biotechnol. Prog.* 1996, *12*, 822-836.

[24] Koegler, W. S., Ivory, C. F. *Journal of Chromatography a* 1996, *726*, 229-236.

[25] Huang, Z., Ivory, C. F. *Anal. Chem.* 1999, *71*, 1628-1632.

[26] Astorga-Wells, J. *Anal. Chem. (Wash.)* 2003, *75*, 5207-5212.

[27] Ross, D., Locascio, L. E. *Anal. Chem.* 2002, *74*, 2556-2564.

[28] Shackman, J. G., Munson, M. S., Kan, C., Ross, D. *Electrophoresis* 2006, *27*, 3420-3427.

[29] Hori, A., Matsumoto, T., Nimura, Y., Ikedo, M. *et al*. *Anal. Chem.* 1993, *65*, 2882-2886.

[30] Polson, N. A., Savin, D. P., Hayes, M. A. *J. Microcolumn Sep.* 2000, *12*, 98-106.

[31] Pacheco, J. R., Chen, K. P., Hayes, M. A. *Electrophoresis* 2007, *28*, 1027-1035.

CHAPTER 2

[1] Lottspeich, F. *Electrophoresis* 2008, *29*, 2449-2450.

[2] Shintani, H., Polonsky, J., Editors. 1997, 737.

[3] Linhardt, R. J., Toida, T. *Science* 2002, *298*, 1441-1442.

[4] Klodzinska, E., Buszewski, B. *Anal. Chem. (Washington, DC, U. S.)* 2009, *81*, 8-15.

[5] Jorgenson, J., Lukacs, K. *Anal. Chem.* 1981, *53*, 1298-1302.

[6] Jorgenson, J., Lukacs, K. *J. Chromatogr.* 1981, *218*, 209-216.

[7] Jorgenson, J., Lukacs, K. *Science* 1983, *222*, 266-272.

[8] Karger, B., Cohen, A., Guttman, A. *J. Chromatogr. -Biomed. Appl.* 1989, *492*, 585-614.

[9] Issaq, H. *Electrophoresis* 1999, *20*, 3190-3202.

[10] Sia, S., Whitesides, G. *Electrophoresis* 2003, *24*, 3563-3576.

[11] Kuehnbaum, N. L., Britz-McKibbin, P. *Chem. Rev.* 2013, *113*, 2437-2468.

[12] Albin, M., Grossman, P. D., Moring, S. E. *Anal. Chem.* 1993, *65*, 489A-497A.

[13] Breadmore, M. C. *Journal of Chromatography a* 2012, *1221*, 42-55.

[14] Breadmore, M., Haddad, P. *Electrophoresis* 2001, *22*, 2464-2489.

[15] Breadmore, M. C. *Electrophoresis* 2007, *28*, 254-281.

[16] Breadmore, M. C., Thabano, J. R. E., Dawod, M., Kazarian, A. A. *et al*. *Electrophoresis* 2009, *30*, 230-248.

[17] Mala, Z., Gebauer, P., Bocek, P. *Electrophoresis* 2011, *32*, 116-126.

[18] Breadmore, M. C., Dawod, M., Quirino, J. P. *Electrophoresis* 2011, *32*, 127-148.

[19] Chen, Y., Lu, W., Chen, X., Teng, M. *Central European Journal of Chemistry* 2012, *10*, 611-638.

[20] Breadmore, M. C., Shallan, A. I., Rabanes, H. R., Gstoettenmayr, D. *et al*. *Electrophoresis* 2013, *34*, 29-54.

[21] Breadmore, M. C., Tubaon, R. M., Shallan, A. I., Phung, S. C. *et al*. *Electrophoresis* 2015, *36*, 36-61.

[22] Mikkers, F. E. P., Everaerts, F. M., Verheggen, T. P. E. M. *Journal of Chromatography A* 1979, *169*, 1-10.

[23] Gebauer, P., Thormann, W., Bocek, P. *J. Chromatogr.* 1992, *608*, 47-57.

[24] Gebauer, P., Thormann, W., Bocek, P. *Electrophoresis* 1995, *16*, 2039-2050.

[25] Aebersold, R., Morrison, H. *J. Chromatogr.* 1990, *516*, 79-88.

[26] Britz-McKibbin, P., Bebault, G., Chen, D. *Anal. Chem.* 2000, *72*, 1729-1735.

[27] Shackman, J. G., Ross, D. *Electrophoresis* 2007, *28*, 556-571.

[28] Giddings, J. C., Dahlgren, K. *Separation Science* 1971, *6*, 345-356.

[29] Ofarrell, P. H. *Science* 1985, *227*, 1586-1589.

[30] Greenlee, R. D., Ivory, C. F. *Biotechnol. Prog.* 1998, *14*, 300-309.

[31] Koegler, W. S., Ivory, C. F. *Biotechnol. Prog.* 1996, *12*, 822-836.

[32] Koegler, W. S., Ivory, C. F. *Journal of Chromatography a* 1996, *726*, 229-236.

[33] Huang, Z., Ivory, C. F. *Anal. Chem.* 1999, *71*, 1628-1632.

[34] Ross, D. *Anal. Chem. (Wash.)* 2002, *74*, 2556-2564.

[35] Shackman, J. G., Munson, M. S., Kan, C., Ross, D. *Electrophoresis* 2006, *27*, 3420-3427.

[36] Hori, A., Matsumoto, T., Nimura, Y., Ikedo, M. *et al*. *Anal. Chem.* 1993, *65*, 2882-2886.

[37] Polson, N. A., Savin, D. P., Hayes, M. A. *J. Microcolumn Sep.* 2000, *12*, 98-106.

[38] Pacheco, J. R., Chen, K. P., Hayes, M. A. *Electrophoresis* 2007, *28*, 1027-1035.

[39] Meighan, M. M., Keebaugh, M. W., Quihuis, A. M., Kenyon, S. M., Hayes, M. A. *Electrophoresis* 2009, *30*, 3786-3792.

[40] Han, J., Chun, M., Riaz, A., Chung, D. *Electrophoresis* 2005, *26*, 480-486.

[41] Meighan, M. M., Vasquez, J., Dziubcynski, L., Hews, S., Hayes, M. A. *Anal. Chem.* 2011, *83*, 368-373.

[42] Beckers, J., Everaerts, F. *J. Chromatogr. A* 1997, *787*, 235-242.

[43] Gebauer, P., Bocek, P. *J. Chromatogr. A* 1997, *772*, 73-79.

[44] Desiderio, C., Fanali, S., Gebauer, P., Bocek, P. *J. Chromatogr. A* 1997, *772*, 81-89.

[45] Gebauer, P., Pantuckova, P., Bocek, P. *Anal. Chem.* 1999, *71*, 3374-3381.

[46] Gas, B., Hruska, V., Dittmann, M., Bek, F., Witt, K. *Journal of separation science* 2007, *30*, 1435-1445.

[47] Squires, T., Bazant, M. *J. Fluid Mech.* 2004, *509*, 217-252.

[48] Yossifon, G., Frankel, I., Miloh, T. *Phys. Fluids* 2006, *18*, 117108.

[49] Takhistov, P., Duginova, K., Chang, H. C. *J. Colloid Interface Sci.* 2003, *263*, 133-143.

CHAPTER 3

[1] Jorgenson, J. W., Lukacs, K. D. *Science* 1983, *222*, pp. 266-272.

[2] Linhardt, R. J., Toida, T. *Science* 2002, *298*, 1441-1442.

[3] Lottspeich, F. *Electrophoresis* 2008, *29*, 2449-2450.

[4] Albin, M., Grossman, P. D., Moring, S. E. *Anal. Chem.* 1993, *65*, 489A-497A.

[5] Giddings, J. C., Dahlgren, K. *Separation Science* 1971, *6*, 345-356.

[6] Righetti, P. G., Drysdale, J. W. *Isoelectric focusing*, Amsterdam, North-Holland Pub. Co. 1976.

[7] Kolin, A. *Proc. Natl. Acad. Sci. U. S. A.* 1955, *41*, 101-10.

[8] O'Farrell, P. H. *Science* 1985, *227*, pp. 1586-1589.

[9] Koegler, W. S., Ivory, C. F. *Journal of Chromatography A* 1996, *726*, 229-236.

[10] Ross, D. *Anal. Chem. (Wash.)* 2002, *74*, 2556-2564.

[11] Astorga-Wells, J. *Anal. Chem. (Wash.)* 2003, *75*, 5207-5212.

[12] Wu, X. *Anal. Chem. (Wash.)* 1998, *70*, 2081-2084.

[13] Wei, W. *Anal. Chem. (Wash.)* 2002, *74*, 3899.

[14] Hori, A., Matsumoto, T., Nimura, Y., Ikedo, M. *et al*. *Anal. Chem.* 1993, *65*, 2882-2886.

[15] McLaren, D. *Anal. Chem. (Wash.)* 2004, *76*, 2298.

[16] Wang, Q., Yue, B., Lee, M. L. *Journal of Chromatography A* 2004, *1025*, 139-146.

[17] Shackman, J. *Anal. Chem. (Wash.)* 2007, *79*, 565-571.

[18] Pacheco, J. R., Chen, K. P., Hayes, M. A. *Electrophoresis* 2007, *28*, 1027-1035.

[19] Polson, N. A., Savin, D. P., Hayes, M. A. *J. Microcolumn Sep.* 2000, *12*, 98-106.

[20] Meighan, M. M., Keebaugh, M. W., Quihuis, A. M., Kenyon, S. M., Hayes, M. A. *Electrophoresis* 2009, *30*, 3786-3792.

[21] Meighan, M. M., Vasquez, J., Dziubcynski, L., Hews, S., Hayes, M. A. *Anal. Chem.* 2011, *83*, 368-373.

[22] Meighan, M. M., Staton, S. J., Hayes, M. A. *Electrophoresis* 2009, *30*, 852-865.

[23] Kenyon, S. M., Meighan, M. M., Hayes, M. A. *Electrophoresis* 2011, *32*, 482-493.

[24] Devasenathipathy, S. *Anal. Chem. (Wash.)* 2002, *74*, 3704-3713.

[25] Devasenathipathy, S., Santiago, J. G., Wereley, S. T., Meinhart, C. D., Takehara, K. *Exp. Fluids* 2003, *34*, 504-514.

[26] Weiss, N. *Electrophoresis* 2011, *32*, 2292-2297.

[27] Han, J. *Electrophoresis* 2005, *26*, 480-486.

[28] He, Y., Lee, H. K. *Anal. Chem.* 1999, *71*, 995-1001.

[29] Pohl, H. *J. Appl. Phys.* 1951, *22*, 869-871.

[30] Chen, K. P., Pacheco, J. R., Hayes, M. A., Staton, S. J. *Electrophoresis* 2009, *30*, 1441-1448.

CHAPTER 4

[1] Albin, M., Grossman, P. D., Moring, S. E. *Anal. Chem.* 1993, *65*, 489A-497A.

[2] Lian, D., Zhao, S., Li, J., Li, B. *Analytical and bioanalytical chemistry* 2014, *406*, 6129-6150.

[3] Dawod, M., Chung, D. S. *Journal of Separation Science* 2011, *34*, 2790-2799.

[4] Breadmore, M. C., Shallan, A. I., Rabanes, H. R., Gstoettenmayr, D. *et al*. *Electrophoresis* 2013, *34*, 29-54.

[5] Chiu, T. *Analytical and Bioanalytical Chemistry* 2013, *405*, 7919-7930.

[6] Kitagawa, F., Otsuka, K. *Journal of Chromatography A* 2014, *1335*, 43-60.

[7] Chien, R. *Electrophoresis* 2003, *24*, 486-497.

[8] Wang, C., Her, G. *Electrophoresis* 2014, *35*, 1251-1258.

[9] Mikkers, F. E. P., Everaerts, F. M., Verheggen, T. P. E. M. *Journal of Chromatography A* 1979, *169*, 1-10.

[10] Burgi, D. S., Chien, R. L. *Anal. Chem.* 1991, *63*, 2042-2047.

[11] Simpson, J.,Steven L., Quirino, J. P., Terabe, S. *Journal of chromatography.A* 2008, *1184*, 504-541.

[12] Giddings, J. C., Dahlgren, K. *Separation Science* 1971, *6*, 345-356.

[13] Meighan, M. M., Staton, S. J., Hayes, M. A. *Electrophoresis* 2009, *30*, 852-865.

[14] Shackman, J. G., Ross, D. *Electrophoresis* 2007, *28*, 556-571.

[15] Polson, N. A., Savin, D. P., Hayes, M. A. *J. Microcolumn Sep.* 2000, *12*, 98-106.

[16] Pacheco, J. R., Chen, K. P., Hayes, M. A. *Electrophoresis* 2007, *28*, 1027-1035.

[17] Meighan, M. M., Keebaugh, M. W., Quihuis, A. M., Kenyon, S. M., Hayes, M. A. *Electrophoresis* 2009, *30*, 3786-3792.

[18] Kenyon, S. M., Keebaugh, M. W., Hayes, M. A. *Electrophoresis* 2014, *35*, 2551-2559.

[19] Sikorsky, A. A., Fourkas, J. T., Ross, D. *Anal. Chem.* 2014, *86*, 3625-3632.

[20] Keebaugh, M. W., Mahanti, P., Hayes, M. A. *Electrophoresis* 2012, *33*, 1924-1930.

[21] Kenyon, S. M., Weiss, N. G., Hayes, M. A. *Electrophoresis* 2012, *33*, 1227-1235.

CHAPTER 5

[1] Giddings, J. C. *J. Chromatogr.* 1960, *3*, 520-523.

[2] Giddings, J. C. *Anal. Chem.* 1963, *35*, 2215-&.

[3] Foret, F., Deml, M., Bocek, P. *J. Chromatogr.* 1988, *452*, 601-613.

[4] Giddings, J. C., Dahlgren, K. *Separation Science* 1971, *6*, 345-356.

[5] Tolley, H. D., Wang, Q. G., LeFebre, D. A., Lee, M. L. *Anal. Chem.* 2002, *74*, 4456-4463.

[6] Kelly, R. T., Woolley, A. T. *Journal of Separation Science* 2005, *28*, 1985-1993.

[7] Ross, D. *Electrophoresis* 2010, *31*, 3650-3657.

[8] Kenyon, S. M., Weiss, N. G., Hayes, M. A. *Electrophoresis* 2012, *33*, 1227-1235.

[9] Meighan, M. M., Keebaugh, M. W., Quihuis, A. M., Kenyon, S. M., Hayes, M. A. *Electrophoresis* 2009, *30*, 3786-3792.

[10] Meighan, M. M., Vasquez, J., Dziubcynski, L., Hews, S., Hayes, M. A. *Anal. Chem.* 2011, *83*, 368-373.

[11] Keebaugh, M. W., Mahanti, P., Hayes, M. A. *Electrophoresis* 2012, *33*, 1924-1930.

[12] Pacheco, J. R., Chen, K. P., Hayes, M. A. *Electrophoresis* 2007, *28*, 1027-1035.

[13] Kenyon, S. M., Keebaugh, M. W., Hayes, M. A. *Electrophoresis* 2014, *35*, 2551-2559.

[14] Giddings, J. C. *Unified separation science*, New York, Wiley 1991.

[15] Karger, B. L., Snyder, L. R., Horváth, C. *An introduction to separation science*, New York, Wiley 1973.

[16] Giddings, J. C. *Sep. Sci. Technol.* 1979, *14*, 871-882.

[17] Taylor, G. *Proceedings of the Royal Society of London Series A-Mathematical and Physical Sciences* 1953, *219*, 186-203.

[18] Culbertson, C. T., Jorgenson, J. W. *Anal. Chem.* 1994, *66*, 955-962.

[19] Hutterer, K., Jorgenson, J. *Anal. Chem.* 1999, *71*, 1293-1297.

APPENDIX A

ADDITIONAL VARIABLES AND DETAILS USED FOR MODELING

Equations used in model

Laminar Flow

Reynolds number (*Re*): $\frac{density \times FlowVelocity \times diameter}{viscosity}$

Laminar regime when *Re* < 2000; creeping (Stokes) flow regime when *Re* << 1

Vector equation representing conservation of momentum (Navier-Stokes)

$$\rho\frac{\partial \mathbf{u}}{\partial t} + \rho(\mathbf{u}\cdot\nabla)\mathbf{u} = \nabla\cdot[-p\mathbf{I}+\boldsymbol{\tau}] + \mathbf{F}$$

For Stokes flow: $\rho(\mathbf{u}\cdot\nabla)\mathbf{u} = 0$

ρ is the density (SI unit: kg/m3)

u is the velocity vector (SI unit: m/s)

p is pressure (SI unit: Pa)

τ is the viscous stress tensor (SI unit: Pa) $\boldsymbol{\tau} = 2\mu\mathbf{S} - \frac{2}{3}\mu(\nabla\cdot\mathbf{u})\mathbf{I}$

F is the volume force vector (SI unit: N/m3)

*C*p is the specific heat capacity at constant pressure (SI unit: J/(kg·K))

T is the absolute temperature (SI unit: K)

q is the heat flux vector (SI unit: W/m2)

Q contains the heat sources (SI unit: W/m3)

S is the strain-rate tensor: $\mathbf{S} = \frac{1}{2}(\nabla\mathbf{u} + (\nabla\mathbf{u})^T)$

μ is dynamic viscosity (SI unit: Pa·s)

Continuity equation representing conservation of mass to describe fluid flow

$$\frac{\partial \rho}{\partial t} + \nabla\cdot(\rho\mathbf{u}) = 0$$

Electric Field

Point form of Ohm's Law for stationary (steady-state) currents in conductive media $\mathbf{J} = \sigma\mathbf{E} + \mathbf{J}_e$

$\mathbf{J}_e$ is an externally generated current density

σ is the electrical conductivity

$\mathbf{E}$ is electric field intensity

Potential $\mathbf{E} = -\nabla V$

V is electric potential (SI unit: V)

Diffusion

Fick's Law and mass balance: $\frac{\partial c}{\partial t} = \nabla \cdot (D\nabla c) + R$

c is the concentration of the species (SI unit: mol/m3)

D denotes the diffusion coefficient (SI unit: m2/s)

R is a reaction (production or consumption) rate expression for the species (SI unit: mol/(m3·s))

Convection

Diffusion mass balance with $\mathbf{u}$ as the velocity vector (SI unit: m/s)

$$\frac{\partial c}{\partial t} + \mathbf{u} \cdot \nabla c = \nabla \cdot (D\nabla c) + R$$

Electrophoretic Migration

Diffusion and convection mass balance with ionic species (i) transport (Nernst-Planck) $\frac{\partial c_i}{\partial t} + \nabla \cdot (-D_i \nabla c_i - z_i u_{\mathrm{m},i} F c_i \nabla \phi + c_i \mathbf{u}) = R_i$

F refers to Faraday's constant (SI unit: A·s/mol)

ϕ denotes the electric potential (SI unit: V)

z_i (dimensionless) is the charge number of the ionic species

$u_{m,i}$ is ionic mobility of species (SI unit: mol·s/kg)

Table A1. Material properties used in model

	Density (kg/m^3)	Relative Permittivity	Conductivity (S/m)	Dynamic Viscosity (Pa*s)	Temperature (K)
Phosphate Buffer	997	80.1	0.0415	0.001	295
Silica Glass	2203	2.09	1×10^{-14}	-	295
Copper	8700	1	5.998×10^{7}	-	295

Meshing of the model

- Hybrid of unstructured free triangular mesh and structured mapped distribution
- Free triangular mesh size ranging from 35 µm (open field) to 0.3 µm (corners)
- Maximum element growth rate 1.1
- Symmetrically distributed element size 1.5 µm laterally (across channel diameter) and 6 µm longitudinally (channel length). Element stretching ratio of 1:4 since laminae are fully developed in this region.
- Boundaries inside channel and along edges adjacent to channel consist of 8 layers.
- Corners are split into elements of no more than 20 degrees.
- No adaptive mesh refinement

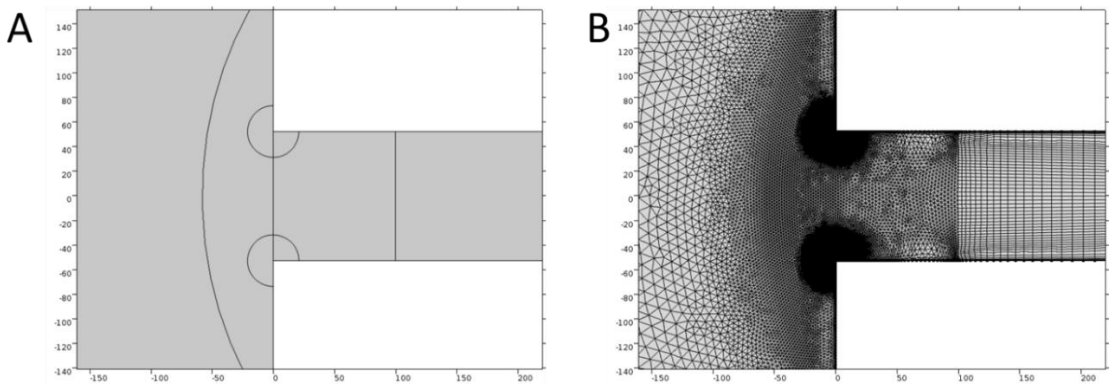

Figure A1. (A) Snapshot of the model entrance with outlined mesh control domains. (B) Specified mesh size was assigned to regions based on predicted steep gradient locations, particularly at the entrance and corners. Note symmetrically distributed mapped elements starting 100 μm inside the channel where fully developed flow and electric fields reside.

APPENDIX B

PUBLISHED PORTIONS

Chapter 3 was published previously in the journal referenced below.

> Keebaugh, M. W., Mahanti, P., Hayes, M. A. *Electrophoresis* 2012, *33*, 1924-1930.

Chapter 4 was submitted to the journal as referenced below.

> Keebaugh, M. W., Hayes, M. A. *Electrophoresis*, submitted

Published portions or portions in preparation for publication were included with the permission of all coauthors.